

T-SiGn tumor reengineering therapy and CAR T cells synergize in combination therapy to clear human lung tumor xenografts and lung metastases in NSG mice

Olmo Sonzogni^a, Daniel E. Zak^a, Maria Stella Sasso^b, Rochelle Lear^b, Alice Muntzer^b, Manuela Zonca^b, Katy West^b, Brian R. Champion^b, and James B. Rottman^a

^aBluebird Bio, Cambridge, MA, USA; ^bPsiOxus Therapeutics Limited, Abingdon, UK

ABSTRACT

Although chimeric antigen receptor (CAR) T cells have emerged as highly effective treatments for patients with hematologic malignancies, similar efficacy has not been achieved in the context of solid tumors. There are several reasons for this disparity including a) fewer solid tumor target antigens, b) heterogenous target expression amongst tumor cells, c) poor trafficking of CAR T cells to the solid tumor and d) an immunosuppressive tumor microenvironment (TME). Oncolytic viruses have the potential to change this paradigm by a) directly lysing tumor cells and releasing tumor neoantigens, b) stimulating the local host innate immune response to release cytokines and recruit additional innate and adaptive immune cells, c) carrying virus-encoded transgenes to “re-program” the TME to a pro-inflammatory environment and d) promoting an adaptive immune response to the neoantigens in this newly permissive TME. Here we show that the Tumor-Specific Immuno-Gene (T-SiGn) virus NG-347 which encodes IFN α , MIP1 α and CD80 synergizes with anti-EGFR CAR T cells as well as anti-HER-2 CAR T cells to clear A549 human tumor xenografts and their pulmonary metastases at doses which are subtherapeutic when each is used as a sole treatment. We show that NG-347 changes the TME to a pro-inflammatory environment resulting in the recruitment and activation of both CAR T cells and mouse innate immune cells. We also show that the transgenes encoded by the virus are critical as synergy is lost in their absence.

ARTICLE HISTORY

Received 22 August 2021
Revised 13 December 2021
Accepted 7 January 2022

KEYWORDS

CAR T cells; T-SiGn oncolytic virus; solid tumor; xenograft; tumor microenvironment; re-program; metastases



Introduction


Chimeric antigen receptor (CAR) T cell therapy has emerged as an important treatment modality for hematologic malignancies. CAR T cells directed against B cell antigens have been tested in the clinic,^{1–10} often inducing long-term remissions in even heavily pre-treated patients^{11–13} and now 5 CAR T cell therapies are on the market for hematologic malignancies.¹⁴ In contrast, CAR T cell therapy has yet to achieve the same depth and reproducibility of response in patients with solid tumors. CAR T cells targeting B7-H3, CEACAM5, CD133, CD171, EGFR, EGFRvIII, FR α , GD2, GPC3, HER2, IL-13Ra2, mesothelin, MUC1, PSMA, ROR1, and VEGF-R2 have been tested in the clinic, but demonstrated limited ability to control disease.^{15–18} Several elements have been hypothesized to contribute to the differences in CAR T clinical efficacy between hematologic malignancies and solid tumors, including a) fewer solid tumor target antigens, b) heterogenous target expression amongst tumor cells, c) poor trafficking of CAR T cells to the solid tumor and d) the solid tumor microenvironment (TME) that is hostile to the function and survival of CAR T cells.^{15,19,20}

Inadequate CAR T cell trafficking to solid tumors (c, above) may be particularly important. In the case of hematologic malignancy, infused CAR T cells immediately mix with circulating neoplastic cells and readily traffic to lymph nodes and bone marrow to interact with tumor cells in those locations. For solid tumors, in contrast, infused CAR T cells disperse

widely in the blood and only a small subset reach the tumor microvasculature. After successful trafficking to the TME, the local microenvironment may impair the function of and/or promote clearance of CAR T cells. A variety of different soluble molecules and immunosuppressive cells (e.g. TGF β , adenosine, regulatory T-cells and myeloid derived suppressor cells) prevent CAR T cell proliferation and function.^{15,19,20} Additionally, immune checkpoint molecules (e.g. PD-L1) expressed by TAMs and tumor cells may also directly impair CAR T cell function.²¹

Thus, to realize successful treatment of solid tumors with CAR T cells, it will be important to find ways to promote CAR T homing to the tumor and reprogram the TME from an immunosuppressive to an immunostimulatory microenvironment. Recently, oncolytic viruses (OVs) have been proposed to be used in combination with CAR T cells for the treatment of solid tumors to address these issues,^{22–24} with most having been genetically engineered or selected to preferentially infect, replicate in, and lyse tumor cells, while not damaging normal cells.²⁵ Conceptually, OVs can mitigate many of the problems that have prevented effective CAR T cell therapy of solid tumors. For example, OV-mediated direct tumor cell lysis directly reduces the solid tumor mass and may make unique tumor associated antigens (TAAs), tumor-specific antigens (TSAs), and/or neoantigens accessible to the host immune system. OV-mediated lysis of tumor cells may also stimulate

CONTACT Brian R. Champion  brian.champion@psioxus.com  PsiOxus Therapeutics Limited, 4-10, The Quadrant, Abingdon Science Park, Barton Lane, Abingdon OX14 3YS, United Kingdom

 Supplemental data for this article can be accessed on the [publisher's website](#).

© 2022 PsiOxus Therapeutics Ltd and Bluebird Bio Inc. Published with license by Taylor & Francis Group, LLC.

This is an Open Access article distributed under the terms of the Creative Commons Attribution-NonCommercial License (<http://creativecommons.org/licenses/by-nc/4.0/>), which permits unrestricted non-commercial use, distribution, and reproduction in any medium, provided the original work is properly cited.

the innate immune response through release of pathogen-associated molecular patterns (PAMPs). The resultant release of proinflammatory cytokines like IFN- α , IFN- γ , TNF- α , IL-6, and IL-12, could then induce anti-viral and anti-tumor immune responses and recruit other immune cells from peripheral lymphoid organs.^{25–27} OV s can also be engineered to deliver novel target antigens to tumor cells (tumor “painting”), thus rendering the cells susceptible to lysis by CAR T cells with receptors specific for that antigen.²⁸ Further, by carrying transgenes that encode cytokines, chemokines, costimulatory or other molecules, OV s can also be designed to actively “reprogram” the TME to a pro-inflammatory state which will recruit and activate additional adaptive and innate immune cells to the TME.²² A number of recent studies have exemplified this, both with fresh human tumor samples cultured *ex vivo*²⁹ and following intra-tumoral dosing in mouse immunocompetent tumor models.^{30,31}

Intra-tumoral dosing of either the OV and/or CAR T cells is either impractical or not feasible at all in many patients and in others only a selected subset of lesions could be dosed. However, the oncolytic group B adenovirus enadenotucirev is stable in blood,³² can be dosed intravenously for selective replication in tumors,^{33,34} and this virus has been developed into a vector (T-SIGn: Tumor-Specific Immunogene) for delivery of transgenes selectively to tumors following IV dosing.³⁴ Here we have evaluated T-SIGn vectors expressing chemokines and immune stimulating transgenes for their impact on CAR T cell therapy in NSG mice bearing human tumor xenografts. We show that T-SIGn vectors a) reprogram the TME toward a pro-inflammatory state, b) enhance CAR T cell and mouse innate immune cell recruitment to the TME, c) synergize with anti-EGFR CAR T cells as well as anti-HER2 CAR T cells to clear A549 xenografts and their metastases, d) this synergy is due, in part, to T-SIGn vector-mediated enhancement of CAR T cell activity and e) the T-SIGn transgene payload is critical for the synergistic effect.

Materials and methods

Cell lines

A549, CT26, HT-29 and HEK293 cell lines were obtained from American Type Culture Collection and cultured in RPMI 1640 media containing 5% fetal bovine sera.

Generation and characterization of T-SIGn viruses enadenotucirev, NG-347 and NG-641

The generation and characterization of enadenotucirev and T-SIGn viral vectors expressing a transgene cassette under control of the virus major late promoter to convey tumor-specific expression have been previously described.^{29,35} NG-641 is a T-SIGn vector that encodes a transgene cassette for expression of an anti-human FAP bispecific T-cell activator (FAP-TAc) as described previously,²⁹ together with human CXCL9, CXCL10 and IFN α . NG-347 has a transgene cassette for expressing human IFN α , MIP1 α and CD80.

Measurement of adenovirus genome copy number and transgene mRNA expression in FFPE tissue samples

Nucleic acid isolation and PCR

Xylenes were used to deparaffinize 10 μ m sections ($n = 2$ per sample) of formalin fixed paraffin embedded (FFPE) tissue prior to total RNA isolation using the RNeasy FFPE Kit (Qiagen), in accordance with a standard protocol with the addition of DNase treatment. RNA concentration was assessed using the Qubit RNA HS Assay Kit (Qiagen). Prior to RNA isolation and following incubation with proteinase K, 20 μ L of lysate from each sample was removed and stored in Buffer ATL. DNA was isolated with the QIAamp DNA FFPE Tissue Kit (Qiagen) using a standard protocol, then quantified using the Qubit dsDNA HS Assay Kit (Invitrogen).

cDNA synthesis was performed using Superscript IV VILO Master Mix (Invitrogen). Quantitative RT-PCR (RT-qPCR) and PCR (qPCR) were performed using primers listed in Table S1 with the Taqman Fast Advanced Master Mix and QuantStudio 3 Real-Time PCR System (Applied Biosystems). PCR conditions were 95°C for 2 mins (for RT-qPCR) or 20 seconds (for qPCR), followed by 40 cycles at 95°C for 1 second and 60°C for 20 seconds. The copies of target genes (IFN α , CD80 and Penton) were calculated using a dilution series (2.5×10^7 to 25 copies per PCR reaction) of linearized plasmid DNA encoding the NG-347 genome sequence. Plasmid DNA was linearized by digest with SbfI (New England Biolabs), then gel extracted using the QIAEX II Gel Extraction Kit (Qiagen), according to the manufacturer’s protocol, prior to quantification as previously described above.

Bulk expression profiling using Nanostring nCounter

Gene expression analysis was conducted using the nCounter Analysis System (Nanostring Technologies) with the PanCancer Immune Profiling Panel codeset and a custom-designed codeset of 17 genes. Each hybridization reaction contained 100ng of RNA in a 5 μ L volume and was supplemented with a pool of reporter and capture probes generated from both codesets prior to incubation, in accordance with the manufacturer’s recommended protocol. The assay background was calculated separately for each sample tested at a 68% confidence level, given by a standard deviation from the mean RNA counts ($\mu + [1 \times \text{SD}]$) of the negative control probes ($n = 8$) in the PanCancer Immune Profiling Panel. The calculated background was subtracted from raw gene expression data, then data were normalized using the NanoStringNorm package (version 1.2.1) in R (version 3.6.1).

Lentiviral vectors and T cell transduction

Anti-EGFR CAR lentiviral vectors (LVV) were replication defective, self-inactivating (SIN), third-generation human immunodeficiency virus type 1 (HIV-1)–based LVV, pseudotyped with the vesicular stomatitis virus–glycoprotein (VSV-G) envelope protein. The vectors used the murine leukemia virus-derived MND promoter³⁶ to drive expression of the chimeric antigen receptor. The anti-EGFR CARs contain a mouse-anti-EGFR single-chain variable fragment (scFv) coupled to the CD8 α hinge and transmembrane

domains, and the intracellular CD137 co-stimulatory (4-1BB) and CD3 ζ chain signaling domains using design principles previously reported.^{37,38} Anti-EGFR CAR LVVs were produced by transient transfection of HEK293T cells with the plasmid transfer vector and packaging plasmids encoding GAG/POL, REV, and VSV-G. Anti-EGFR CAR LVV was purified via chromatography and formulated before storage at $\leq -65^\circ\text{C}$.

To initiate T-cell cultures, bulk PBMCs were activated with soluble human anti-CD3, clone OKT3 (Miltenyi Biotec), and human anti-CD28, clone 15E8 (Miltenyi Biotec), in T-cell growth media (TCGM) consisting of X-VIVO™ 15 media (Lonza) supplemented with 5% human serum, type AB (Valley Biomedical), 2 mM of GlutaMAX™-I (Gibco), 10 mM of HEPES buffer solution (Gibco), and 250 IU/mL of recombinant human interleukin-2 (rhIL-2; CellGenix GmbH) with culture at 37°C in a 5% CO₂ incubator. The next day, cells were transduced with LVV (multiplicity of infection [MOI] = 20), and T cells were expanded for 7–15 days at a concentration of $0.3\text{--}0.5 \times 10^6$ cells/mL. Untransduced (UTD) T-cell controls compared in each individual study were from donor-matched parallel cultures.

Anti-HER2 CAR T cells with a human HER2-specific ScFv linked to an intracellular CD137 & CD3 ζ signaling domain and co-expressing green fluorescent protein (GFP) were purchased from ProMab (PM-CAR1064, ProMab, Richmond, CA, USA). Tumor-specific killing activity of these CAR T cells was confirmed by coculturing with A549 tumor cells (HER2 positive) or the CT26 mouse colorectal tumor cell line as a negative control (Figure S7). Tumor cell viability after CAR T cell addition was monitored using an xCELLigence Real Time Cell Analysis instrument (Agilent, Santa Clara, CA, USA).

To detect cell surface anti-EGFR CAR expression, T cells were labeled with LIVE/DEAD® Fixable Near-IR Dead Cell Stain Kit (Molecular Probes) according to the manufacturer's instructions to exclude dead cells and followed by incubation with Biotin-Goat Anti-Mouse IgG (H + L; Molecular Probes) for 20 min at 4°C . Following a wash step, the cells were incubated with R-phycoerythrin (PE) streptavidin and CD3 PerCP-Cy5.5, clone SK7 (BD Pharmingen), for 20 min at 4°C and fixed. Samples were acquired on an LSRFortessa™ Cell Analyzer (BD Biosciences) and analyzed using FlowJo Single Cell Analysis Software v9.0 (FlowJo, LLC). Expression of HER2-specific CAR molecules was similarly assessed by flow cytometry using a biotinylated AffiniPure F(ab')₂ fragment goat anti-human IgG, F(ab')₂ fragment-specific antibody (Jackson ImmunoResearch Ely, Cambridgeshire, United Kingdom) followed by PE-Streptavidin.

Vector copy number (VCN) was determined using qPCR, as described previously.³⁹ Briefly, gDNA was isolated from transduced T cells using Quick-gDNA™ MiniPrep kit (Zymo Research Corp). qPCR reactions were run on the StepOnePlus™ Real-Time PCR System (Applied Biosystems) using TaqMan® Universal Master Mix II, no UNG (Applied Biosystems), according to the manufacturer's instructions. TaqMan® Copy Number Reference Assay, human RNase P (Applied Biosystems), and custom psi gag primer/probe set (Life Technologies) were run in multiplex. Analysis was

performed using StepOne Software v2.2 (Applied Biosystems) using the $\Delta\Delta\text{Ct}$ method. The average VCN was calculated by normalizing psi gag copies to RNaseP copies in diploid cells.

Mouse tumor xenograft studies

All in vivo studies were conducted with the approval and oversight of the bluebird bio Institutional Animal Care and Use Committee. 6–10 week old NOD-SCID- $\gamma^{-/-}$ (NSG) mice were injected subcutaneously with 5×10^6 A549 human tumor cells on the flank on day ~21. Tumor xenograft length, width, and height were measured with calipers bi-weekly until the average size was approximately $100\text{--}150\text{mm}^3$ (studies with EGFR CAR T cells) or $100\text{--}350\text{mm}^3$ (studies with HER-2 CAR T cells) calculated as length \times width \times height \times 0.52 = Tumor Volume (mm³).⁴⁰ Animals were subsequently randomized into treatment groups (n = 5–10 animals/group depending upon the experiment) to achieve an equivalent average tumor size across groups at the beginning of treatment. Bi-weekly tumor measurements continued as described above for the duration of the experiment. Animals were humanely euthanized when tumor volume exceeded 500mm^3 or on a pre-determined study termination date. Biweekly tumor measurements were compared between groups using multiple T-tests (GraphPad Prism v 8.0.1). Tumor xenografts and lungs collected at various times during experiments were fixed in 10% neutral buffered formalin for 24 hours, processed and embedded in paraffin.

Immunohistochemistry

To detect adenovirus capsid antigen, tumor xenograft or lung FFPE samples were sectioned at $5\ \mu\text{m}$, and stained on the Ventana Ultra robot (Roche Diagnostics). Sections were dewaxed, target retrieved, digested with Protease 2 (Roche cat# 760–2019), and then sequentially incubated with protein block, anti-adenovirus capsid antibody (EMD Millipore cat# MAB8052) or isotype control (Abcam cat# ab18443) at room temperature for 60 minutes, linking rabbit-anti-mouse antibody (abcam #ab125907), OmniMap anti-rabbit -HRP antibody (Roche cat# 760–4311) and then ChromoMap DAB kit (Roche cat# 760–159).

To enumerate lung metastases, the mouse lungs and trachea were embedded in paraffin en bloc, serially sectioned to the level of the mainstem bronchus and a single $5\ \mu\text{m}$ FFPE section was cut at this level. Lung sections were dewaxed, target retrieved, and then sequentially incubated with protein block followed by anti-pan-cytokeratin antibody (Cell Signaling pan-cytokeratin #4545) or isotype control (BD Pharmingen #554121) at room temperature for 120 minutes. Subsequently, endogenous peroxidase was blocked (Biocare Medical #PX968NMM) and then slides were incubated for 30 minutes at room temperature with goat-anti-mouse HRP polymer (Biocare Medical #MHRP520L). Finally, slides were developed for 5 minutes at room temperature with DAB (Biocare Medical #DBC859L10). Subsequently, slides were digitally scanned (Pannoramic Flash III, 3Dhistech), the digital images were reviewed (CaseViewer software, 3Dhistech) and pulmonary metastases were manually enumerated.

To demonstrate tumor vascularity, tumor xenograft FFPE samples were sectioned at 5 μm , and stained on the Ventana Ultra robot (Roche Diagnostics). Sections were dewaxed, target retrieved and then sequentially incubated with protein block, rat-anti-mouse CD-31 antibody (Dianova cat#DIA-310) or isotype control (Abcam cat #ab18412) at room temperature for 60 minutes, linking rabbit-anti-rat antibody (Jackson Immuno cat # 312-005-003), OmniMap anti-rabbit -HRP antibody (Roche cat# 760-4311) and then Discovery Purple chromagen (Roche cat# 760-229).

Digital Spatial Profiling (DSP)

Tumor xenograft FFPE samples were sectioned at 5 μm , dewaxed, target retrieved, digested with proteinase K, post-fixed, and then incubated overnight with GeoMx Cancer Transcriptome Atlas (CTA) RNA detection probes (Nanostring, Seattle, WA) as previously described.⁴¹ Stringent washes were performed followed by the incubation of fluorescently labeled antibodies against smooth muscle actin, pan cytokeratin, fibroblast activation protein, human CD45 and/or murine CD11b and a nuclear DAPI stain for use as morphology markers. User-defined regions of interest (ROI) were then selected on the GeoMx Digital Spatial Profiling (DSP) instrument (Nanostring, Seattle, WA) through region-specific cleavage and collection of the photocleaved indexing oligonucleotides. Cleaved indices were then quantified via Next Gen Sequencing technology generating digital quantification of RNA expression with spatial context.

Bioinformatics analysis

Analysis of Digital Spatial Profiling (DSP) data: Gene-level data normalized by the Nanostring “Q3” method was used in all analyses involving DSP. The Q3 normalization method uses the top 25% of expressed genes within a ROI to scale expression so that expression patterns across ROIs may be compared.

DSP data analysis of tumor xenografts collected at the time of CAR T cell infusion (6 days after the 1st NG-347 infusion): DSP was performed using the Cancer Transcriptome Atlas probe library for a total of 24 ROIs: 12 ROIs from a tumor xenograft from a mouse treated with NG-347 and 12 from a tumor xenograft from a control mouse. Two ROIs from the tumor xenograft from the NG-347-treated mouse exhibited concordant exceptionally high expression of the NG-347-encoded transgenes CCL3 (over 40X median) and CD80 (over 3X median) and were designated as “high transgene” ROIs. Note that the NG-347-encoded IFNA2 transgene was not detectable in this first DSP analysis because the IFNA2 probes detect only untranslated regions of the gene that are not expressed in the construct. Prior to testing for differential expression, genes from the Q3 normalized dataset were filtered to exclude: (1) negative control probes, (2) CCL3 and CD80, and (3) genes exhibiting only low-level expression, which was defined as having 90% quantiles of Q3 normalized expression $\leq 2^6$. This reduced the testable gene set from 1811 to 1767 genes. Gene expression testing was then performed using the Kendall Tau rank correlation test to identify genes with expression levels that varied between ROIs in a manner significantly associated

with extent of oncolytic virus replication, which was defined in terms of three ordered levels: 1 = *no viral replication*: the tumor xenografts from control mice, 2 = *moderate replication*: ROIs from tumor xenografts of NG-347 treated mice that did not exhibit exceptional transgene expression, and 3 = *high replication*: ROIs from tumor xenografts of NG-347 treated mice with exceptional CCL3 and CD80 transgene expression. Testing was performed using the package *Kendall* in R, p-values were adjusted for multiple testing using the Benjamini-Hochberg false discovery rate (FDR) method, and genes with $\text{FDR} < 0.05$ and average $|\log_2(\text{fold-change})| \geq 0.5$ between ROIs from control mice and moderate or high replication ROIs were selected for subsequent analysis. This analysis yielded 110 and 102 genes positively and negatively associated with oncolytic virus replication, respectively. Testing for over-representation of pathways and functional annotations within these replication-associated groups of genes was performed using Fisher’s Exact test and the following gene sets that were accessed through the R package *msigdb*: Hallmarks,⁴² Reactome,⁴³ KEGG,⁴⁴ and Biocarta. At $\text{FDR} < 0.01$ and requiring at least six overlapping genes, 15 pathways were significantly over-represented within genes positively associated with viral replication, and 10 pathways were significantly over-represented within genes negatively associated with viral replication. Heatmap visualizations of significant genes and pathway associations were made using the R package *pheatmap*.

DSP data analysis of tumor xenografts collected 7 days after CAR T cell infusion (13 days after the 1st NG-347 infusion): DSP was performed for a total of 71 ROIs: 48 ROIs from tumor xenografts from two mice treated with NG-347 in combination with CAR T cells and 23 ROIs from tumor xenografts from two mice treated with CAR T cells alone. For these assays, the Cancer Transcriptome Atlas probe library was appended with additional probes to detect the NG-347-encoded IFNA2 transgene and mouse-specific probes for *Itgax* (Cd11c), *Adgre1* (F4/80), and *Hprt* to detect infiltration of murine cells into the tumor xenograft. Each ROI was then scored in terms of T cell infiltration and oncolytic virus transgene expression (a surrogate for viral replication) using the \log_2 average of relevant gene sets. Five T cell-specific genes (*PTPRC/CD45*, *CD247/CD3Z*, *CD3D*, *CD3E*, *TRAC*, and *TRBC1/2*) were used to compute the T cell infiltration score, and all three transgenes encoded by NG-347 (*CCL3/MIP1a*, *CD80*, and *IFNA2*) were used to compute the transgene score. T cell and transgene scores were each then binned into three discrete levels in the following manner: (1) *T cell infiltration*: ROIs from both tumor xenograft groups exhibited largely comparable distributions of T cell scores except for a subset of ROIs in the NG-347 + CAR T cell group with scores that were very high. Receiver operating characteristic (ROC) analysis was used to identify a threshold that discriminated these high T cell ROIs from the others, and then partition around medoids (PAM) was used to cluster the remaining ROIs into low vs. medium T cell infiltration groups. (2) *Transgene expression*: ROC analysis was first used to find a transgene score threshold that discriminated NG-347 + CAR T cell tumor xenograft ROIs from CAR T cell tumor xenograft ROIs (where all transgene expression would be due to background endogenous levels). A \log_2 transgene score of 6.22 discriminated the two groups with 100% specificity and 92% sensitivity, indicating that oncolytic

virus replication was absent from approximately 8% of ROIs from NG-347+ CAR T cell tumor xenografts. PAM was then used to cluster the remaining NG-347 + CAR T cell ROIs into medium vs. high transgene expression groups.

Results

Characterization of T-SIGn virus activity

Prior to proceeding with in vivo experiments, the various T-SIGn viruses used in this study (enadenotucirev, NG-347 and NG-641) were characterized in vitro to assess oncolytic activity and transgene expression. First, the oncolytic activity of NG-347 on A549 cells was demonstrated to be equivalent to that of the parental vector, enadenotucirev (Figure S1). Additionally, permissive A549 cells infected with NG-347 were demonstrated to express the human transgenes encoding MIP1 α (Figure S2, panel A), IFN α (Figure S2, panel B), and CD80 (Figure S3) whereas non-permissive MRC-5 cells did not. Enadenotucirev and NG-347 did not directly stimulate T cells as neither human CD4 nor CD8 T cells upregulate CD25 or CD69 upon exposure to the viruses (Figure S4), but when co-cultured with virus-infected A549 cells, T-cells were activated to upregulate CD69 and IFN γ

in response to NG-347 (Figure S5 panels A and B, respectively). Similar to NG-347, the oncolytic activity of NG-641 on HT-29 cells was demonstrated to be equivalent to that of the parental vector, enadenotucirev (data not shown) and all four NG-641 transgene products were expressed (Figure S6).

Optimization of T-SIGn virus route of administration and dosing schedule

First, we evaluated the level of viral vector delivery to the TME following intravenous (IV) dosing or intra-tumoral (IT) dosing. Groups of mice bearing bilateral A549 human tumor xenografts were treated either with three IV injections of enadenotucirev virus particles (the T-SIGn empty vector) or PBS on Days 0, 3 and 5 or a single IT injection of enadenotucirev virus particles or PBS control into each tumor on Day 0 (Figure 1a). Tumors were subsequently collected from the animals on Days 6 and 14 (IV route) or Day 4 (IT route). One of the bilateral tumors from each animal was snap frozen in liquid nitrogen for viral load analysis via qPCR and the second tumor from each animal was formalin-fixed and paraffin embedded (FFPE). FFPE sections of the tumors were subsequently stained with H&E and via IHC to detect adenovirus capsid protein expression. A549 tumors grow

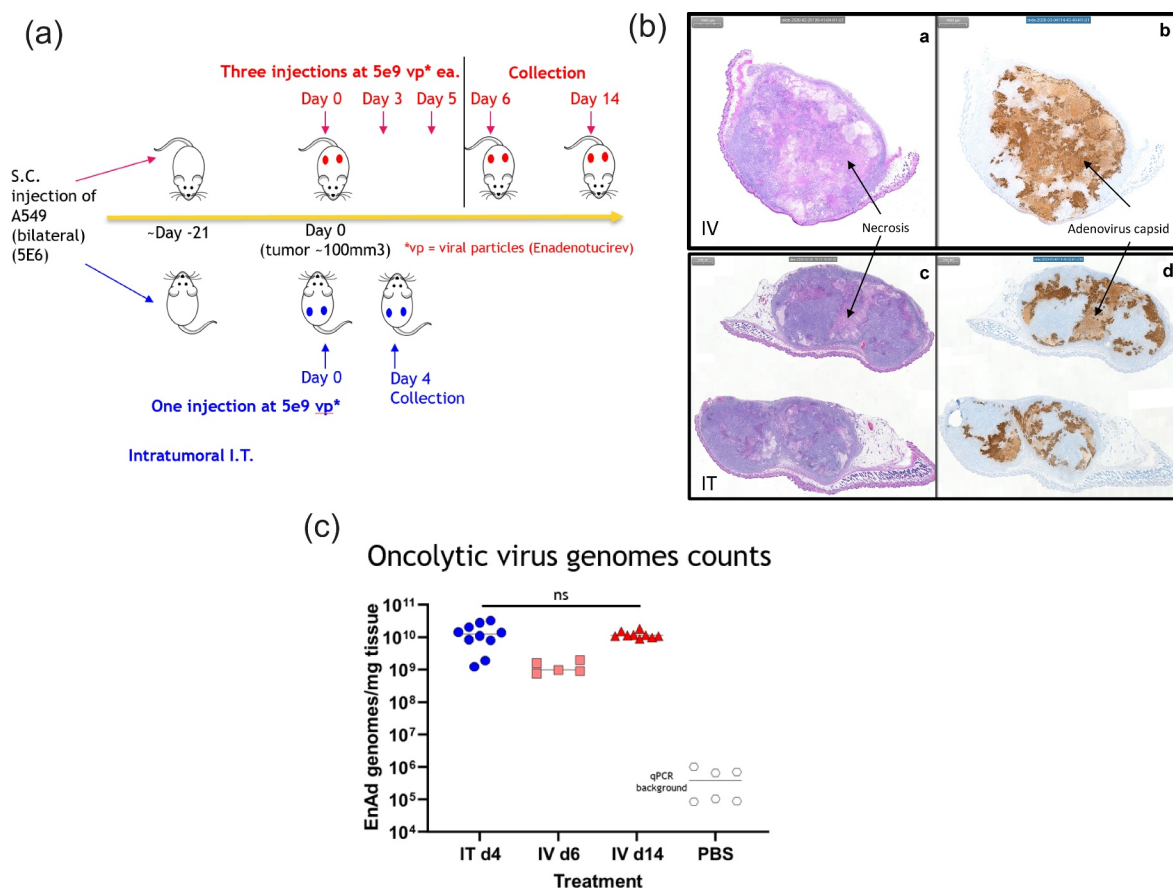


Figure 1. Evaluation of the level of enadenotucirev delivery to subcutaneous A549 tumors in NSG mice. a) NSG mice bearing bilateral A549 tumors were treated with either three intravenous (IV) doses of 5×10^9 enadenotucirev virus particles (vp) on Days 0, 3 and 5 or a single 5×10^9 vp intra-tumoral (IT) dose on Day 0. Tumors were collected on Days 6 and 14 (IV route) or Day 4 (IT route) and one of the bilateral tumors from each mouse was snap frozen for molecular analysis. The other tumor from each mouse was fixed in formalin, processed to paraffin block (FFPE) and sectioned for histologic evaluation. b) Sections of the FFPE tumors were stained with H&E and via IHC to detect adenovirus capsid protein expression. Analysis of the H&E tumor sections from animals treated with enadenotucirev via either the IV or IT routes yielded large areas of A549 tumor necrosis (Arrows, Panels A and C, respectively) which contained robust adenovirus capsid protein expression (Arrows, Panels B and D, respectively). c) The snap frozen tumor from each animal was subsequently evaluated via qPCR to enumerate virus genomes per mg of tissue and the IV administration route (Day 14) yielded a roughly equivalent virus load to the IT administration route (ns = no significant difference between groups).

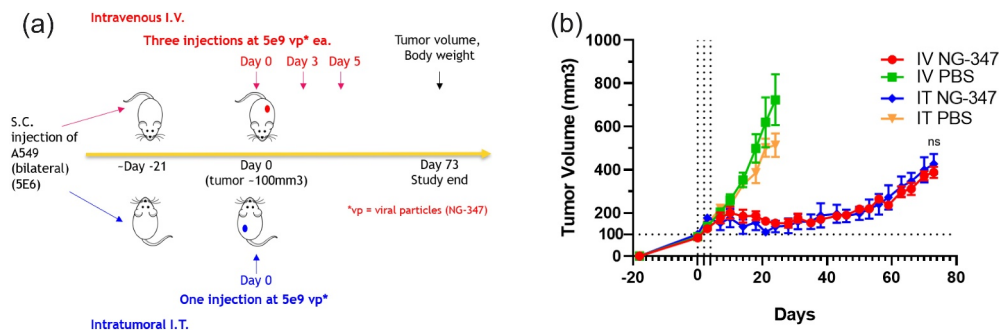


Figure 2. Impact of NG-347 delivery via the IT vs IV route on subcutaneous A549 tumor growth in NSG mice. a) Animals bearing single A549 tumors were treated either with a single IT injection of 5×10^9 NG-347 virus particles or PBS as comparator controls on Day 0 or with three IV injections of 5×10^9 NG-347 virus particles or PBS on Days 0, 3 and 5. b) Tumor volume was measured biweekly through Day 73. IV and IT administration provided equivalent levels of tumor growth suppression, supporting the intravenous dosing route for subsequent studies (ns = no significant difference between groups).

relatively quickly, and larger tumors often contain necrotic regions which may originate in areas of low vascular density (Figure S7). Evaluation of the H&E slides showed that both IV and IT enadenotucirev administration yielded large areas of tumor necrosis (Figure 1b, Panels a and c, respectively) which contained robust adenovirus capsid protein expression (Figure 1b, Panels b and d, respectively), indicating that the necrosis was caused by the virus rather than insufficient vascularity. Likewise, the snap frozen tumors were subsequently evaluated via qPCR to enumerate virus genomes per mg of tissue and the IV administration route (Day 14) yielded a roughly equivalent virus load to the IT administration route (Figure 1c).

Because our ultimate goal was to use the NG-347 T-SIGN vector (which encodes IFN α , MIP1 α and CD80) for our OV + anti-EGFR CAR T cell combination studies, we next studied the impact of this virus variant on tumor xenograft growth when delivered as a single agent. Animals bearing single A549 tumor xenografts were treated either with a single IT injection of NG-347 virus particles or PBS as comparator control on Day 0 or with three IV injections of NG-347 virus particles or PBS on Days 0, 3 and 5 (Figure 2a), following previously optimized dosing regimens for T-SIGN viruses, which broadly align to those used in clinical studies.^{34,35,45} Tumor volume was measured biweekly through Day 73. IV and IT administration provided equivalent levels of tumor growth suppression (Figure 2b), supporting the intravenous dosing route for subsequent studies. Because three intravenous injections of virus caused robust inhibition of tumor growth, potentially impeding our ability to demonstrate any additive antitumoral activity of CAR T cells delivered in combination, we chose to move forward with only two IV doses of NG-347 virus particles delivered on Days 0 and 3 and then treat with anti-EGFR CAR T cells on Day 6 for subsequent A549 tumor xenograft studies.

T-SIGN virus NG-347 synergizes with anti-EGFR CAR T cells to clear primary tumors and pulmonary metastases

To determine if NG-347 would synergize with anti-EGFR CAR T cells to clear A549 tumors and their pulmonary metastases, tumor-bearing NSG mice were treated IV with NG-347 or vehicle and then treated with various doses of anti-EGFR CAR T cells, untransduced T cells or vehicle via the intravenous route on Day 6 (Figure 3a and Table 1). Tumors were collected from satellite

animals treated with vehicle or NG-347 on Day 6 prior to CAR T cell administration and processed to paraffin block. For the animals remaining in the study, tumor volume was measured biweekly and lungs were collected from all animals at the time of euthanasia to enumerate metastases.

We first determined the extent of NG-347 delivery to and replication within the TME at the time of CAR T treatment (Day 6) via immunohistochemistry. As shown in Figure 3b, tumors from the satellite animals that were treated with NG-347 had focal regions of viral capsid immunoreactivity scattered throughout the A549 TME, thus demonstrating that the virus was present and replicating within the TME at the time of CAR T cell delivery.

The tumor growth curves from this experiment are illustrated in Figure 3c. When used as a single agent, NG-347 significantly inhibited tumor growth, but did not clear A549 tumors (Figure 3c, Panel B). However, when animals were pre-treated IV with NG-347 virus particles on Days 0 and 3 and then treated IV with anti-EGFR CAR T cells on Day 6, the two treatment modalities synergized. The combination of NG-347 + high dose anti-EGFR CAR T cells completely cleared the tumors (10/10 animals) and was significantly more effective than either NG-347 alone or the same dose of anti-EGFR CAR T cells delivered as a single agent, which cleared only 2/5 tumors (Figure 3c, Panels C and D). Likewise, the combination of NG-347 + mid-dose anti-EGFR CAR T cells cleared the tumors in 8/10 animals and was significantly more effective than either NG-347 alone or the same dose of anti-EGFR CAR T cells delivered as a single agent (Figure 3c, Panels E and F). Finally, even the combination of NG-347 + low dose anti-EGFR CAR T cells was significantly more effective than either NG-347 alone or the same dose of anti-EGFR CAR T cells delivered as a single agent (Figure 3c, Panels G and H), but the tumors ultimately began to grow back (only 2/10 animals treated with the combination were tumor free at the end of the study). Untransduced T cells delivered as a single agent at 25.2×10^6 cells/mouse had no impact on tumor growth (Figure 3c, Panel A). Interestingly, when animals were pre-treated IV with NG-347 virus particles on Days 0 and 3 and then treated IV with the same dose of UTD cells on Day 6, the UTD cells partially inhibited the anti-tumor activity of NG-347 (Figure 3c, Panel A).

To determine if the various treatments had an impact on A549 lung metastases, a single $5 \mu\text{m}$ FFPE section of lung from each animal cut at the level of the mainstem bronchus was

stained for human pan-cytokeratin via IHC and examined microscopically to enumerate metastases. Animals treated with the vehicle control had an average of 12.0 ± 2.1 metastases and animals treated with UTD cells as a sole therapy had an average of 17.4 ± 6.7 metastases. Animals treated with NG-347 as a sole agent or NG-347 followed by UTD cells experienced a significant reduction in the number of metastases as compared to the vehicle control (2.3 ± 1.0 metastases and 2.4 ± 1.0 metastases, respectively). Animals treated with the high or mid-dose anti-EGFR CAR T cells, either as a sole therapy or in combination with NG-347 did not have any lung metastases. In contrast, animals treated with the low dose of anti-EGFR CAR T cells as a sole agent had lung metastases, but the number was significantly reduced (2.6 ± 1.4 metastases), as compared to the vehicle control. Finally, animals treated with

the combination of NG-347 + and low dose anti-EGFR CAR T cells had a significant reduction of lung metastases (0.3 ± 0.2 lung metastases) as compared to animals treated with that dose of anti-EGFR CAR T cells as a sole agent. Interestingly, the number of metastases in the NG-347 + low dose anti-EGFR CAR T group was decreased as compared to the number of metastases in animals treated with NG-347 alone, but the difference was not significant. Thus, NG-347 is able to substantially reduce the number of lung metastases when used as a sole agent and CAR T cells synergize with the virus to cause a further (albeit statistically insignificant) reduction in lung metastasis burden. It is interesting to note that in the few mice treated with NG-347 that had remaining lung metastases, we could often identify adenovirus replication localized to the metastatic site via IHC (Figure S8).

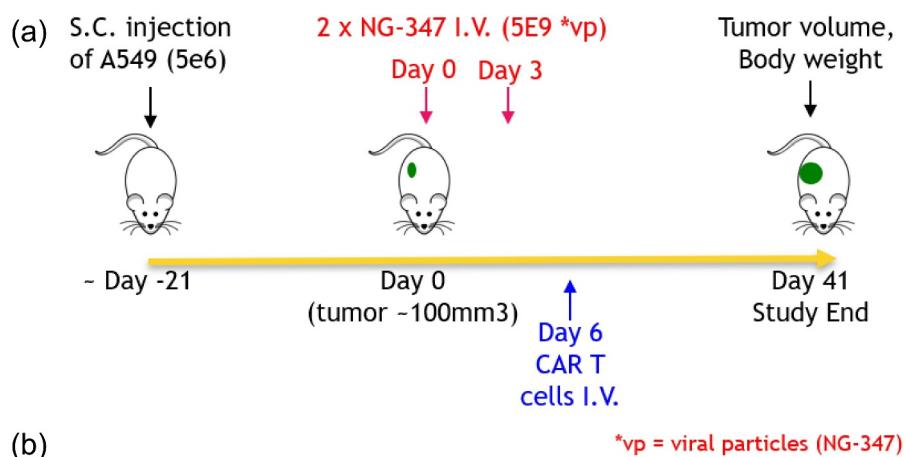


Figure 3a. T-SIGN virus NG-347 synergizes with anti-EGFR CAR T cells to clear primary tumors and pulmonary metastases. a) A549 tumor-bearing NSG mice were treated IV with NG-347 or vehicle on Days 0 and 3 and then treated with various doses of anti-EGFR CAR T cells, untransduced T cells (UTD) or vehicle via the intravenous route on Day 6. b) FFPE tumors collected from satellite animals treated with vehicle control or NG-347 on Day 6 prior to CAR T cell administration were stained by IHC to detect adenoviral capsid. Tumors from animals that were treated with NG-347 had focal regions of viral capsid immunoreactivity (brown) scattered throughout the TME and tumor sections from animals treated with vehicle control were unstained (not shown). c) T-SIGN virus NG-347 synergizes with anti-EGFR CAR T cells to clear primary tumors (complete data from animals treated with high dose anti-EGFR CAR T or UTD cells and controls is presented in Panel a). Panel b compares tumor growth in mice from the untreated (vehicle) group with those mice treated with NG-347; Panels c-d show paired treatment comparisons for NG-347 combined with the high dose anti-EGFR CAR T cells vs NG-347 alone or vs anti-EGFR CAR T cells alone, respectively; Panels e-f compare the effect of NG-347 combined with the medium dose of anti-EGFR CAR T cells vs NG-347 alone or vs anti-EGFR CAR T cells alone, respectively; Panels g-h compare the effect of NG-347 combined with the low dose of anti-EGFR CAR T cells vs NG-347 alone or vs anti-EGFR CAR T cells alone, respectively. d) To determine if the various treatments had an impact on A549 lung metastases, a single $5 \mu\text{m}$ FFPE section of lung from each animal cut at the level of the mainstem bronchus was stained for human pan-cytokeratin via IHC and examined microscopically to enumerate metastases. Symbols indicate significance level from one-sided t-test comparing the indicated groups: *, # indicate $p < .05$ or 0.01 , respectively.

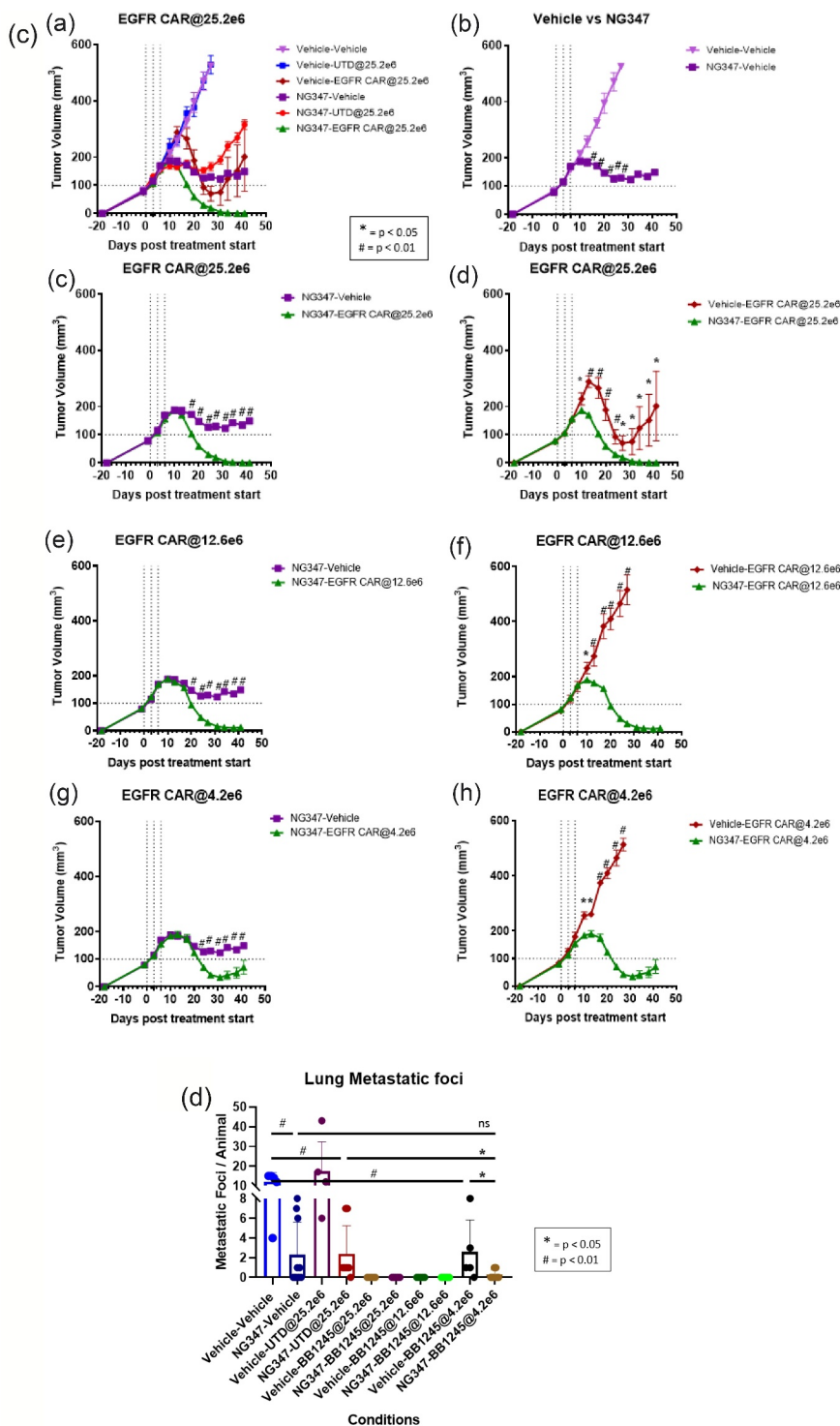


Figure 3b. Continued

T-SIGn virus NG-347 “re-programs” the A549 TME to a proinflammatory state

One of our hypotheses was that NG-347 would “re-program” the TME to a pro-inflammatory state, thereby enhancing CAR T cell recruitment and activation. To study the impact of NG-347 replication on the A549 TME transcriptome, serial 5 μm

FFPE sections of tumors collected from the satellite vehicle and NG-347 treatment groups described above on Day 6 (n = 1 tumor from each group) were subjected to adenovirus capsid IHC and Digital Spatial Profiling (DSP) transcriptional analysis (Figure 4a). Adenovirus-positive ROIs containing virus were confirmed by markedly elevated expression of human MIP1α and CD80 transcripts (transgene payloads of NG-347) and

were subcategorized into virus high and virus low samples based upon expression levels, thus yielding 3 groups: Control (green), NG-347 low (pink) and NG-347 high (blue). This analysis identified 110 transcripts that were significantly positively associated with NG-347 levels that we then tested for over-representation of inflammatory pathways (Figure 4b). Some of the most strongly enriched pathways were related to IFN α and IFN γ response, antigen processing and presentation, cytokine signaling, inflammation, and hypoxia.

Collectively, these data show that a) NG-347 re-programs the A549 tumor xenograft TME to a pro-inflammatory state and b) that the proinflammatory state is associated with enhanced anti-tumor efficacy both at the primary tumor and sites of distant metastases.

The synergistic anti-tumor effect of NG-347 + anti-EGFR CAR T cells is dependent upon virus dose

Having demonstrated that NG-347 reprogrammed the A549 TME to a proinflammatory environment and shown that anti-EGFR CAR T cells synergized with NG-347 to clear the tumors and their metastases, we next wanted to a) make sure that the results were reproducible, b) study the impact of virus dose on anti-tumor efficacy and c) study the impact of NG-347 treatment on CAR T cell activation within the A549 tumor TME. Accordingly, A549 tumor-bearing mice were treated IV with either vehicle or various doses of NG-347 and then either with vehicle or a constant dose of UTD or anti-EGFR CAR T cells (Figure 5a). Animals treated with NG-347 as a sole agent experienced a dose-dependent reduction in tumor burden as compared to the vehicle control animals (Figure 5b, Panel B). The combination of high dose NG-347 + anti-EGFR CAR T cells cleared the tumors in 4/5 animals and was significantly more effective than the same doses of NG-347 or anti-EGFR CAR T cells delivered as a single agent (Figure 5b, Panels C and D). Likewise, the medium dose of NG-347 + anti-EGFR CAR T cells reduced the tumor burden significantly more than the same doses of NG-347 or anti-EGFR CAR T cells delivered as a single agent (Figure 5b, Panels E and F). Finally, although the combination of low dose NG-347 + anti-EGFR CAR T cells was significantly more effective than anti-EGFR CAR T cells alone, the combination was only slightly more effective for a short period of time than the same dose of NG-347 delivered as a single agent (Figure 5b, Panels G and H). Interestingly, as observed in the last experiment, the combination of UTD cells + high dose NG-347 was less efficacious than high dose NG-347 delivered as a single agent (Figure 5b, Panel A).

NG-347 enhances the recruitment and activation of anti-EGFR CAR T cells resulting in their improved efficacy against A549 tumor xenografts

To evaluate the overall effects of NG-347 and anti-EGFR CAR T cells either individually or in combination on the TME, bulk Nanostring nCounter gene expression profiling of mRNA extracted from tumor FFPE sections (Day 13) from the satellite animals mentioned above was undertaken. Animals treated with the combination of NG-347 + anti-EGFR CAR T cells

preferentially exhibited robust expression of T cell activation (Figure 6a) and inflammatory chemokine (Figure 6b) genes, which was lacking in the other treatment groups, indicating strongly synergistic T cell and recruitment and activation.

To further investigate how the oncolytic virus + CAR T cell combination synergistically impacted intra-tumoral immune cell recruitment and activation, we applied DSP transcriptional analysis to compare tumors from mice treated with anti-EGFR CAR T alone to tumors from mice treated with NG-347 + anti-EGFR CAR T cells (Figure 6c). NSG mice are a strongly immunodeficient mouse strain, lacking T cells, B cells and NK cells, allowing the growth of human tumor xenografts, but these mice still retain innate myeloid immune cells thus allowing us to investigate the effect of NG-347-CAR T cell combination on host myeloid cell recruitment.

We first scored each spatial region of interest (ROI) in the DSP dataset according to a virus transgene score (based on NG-347 transgenes) and a T cell infiltration score (based on expression of T cell markers) (Figure 6d). This analysis revealed marked heterogeneity across spatial regions of the tumors, allowing stratification of the ROIs in terms of NG-347 transgene expression and T cell infiltration into 3 discreet levels for each factor (Figure 6d). Generally, T cell infiltration increased as the virus infection increased, with an apparent artefactual decrease in T cells in the ROIs with highest virus transgene scores likely due to substantial necrosis. Assessing how cytotoxic effector molecule expression varied between the ROI groupings revealed that both Granulysin and Granzyme-B were preferentially over-expressed in ROIs with moderate-to-high virus transgene expression and high overall T cell infiltration, but not ROIs lacking virus transgene expression (Figure 6e). Over-expression of these effector molecules may result from higher T cell infiltration overall and/or greater cytotoxic activation of the T cells within the ROIs. We therefore also assessed expression Granulysin and Granzyme-B relative to the overall T cell infiltration score for each ROI (figure 6f) and this revealed that in tumor regions with moderate-to-high virus replication levels not only exhibit higher cytotoxic effector molecule levels overall, but also higher levels of these markers relative to the amount of infiltrating T cells. NG-347 in combination with anti-EGFR-CAR T cells therefore appears to promote both recruitment of CAR T cells to the tumor and cytotoxic skewing of intra-tumoral CAR T cells.

Differential expression analysis across the stratified ROIs also revealed preferential expression of murine innate immune cells into ROIs exhibiting moderate-to-high virus transgene expression and high T cell infiltration (Figure 6g), as measured by mouse-specific probes for DCs (mCD11c) and macrophages (mF4/80). This suggested that the NG-347-driven inflammatory mechanisms leading to increased T cell infiltration could also be recruiting the innate arm of residual immunity of NSG mice. To test whether murine innate immune cells co-infiltrated the tumors alongside human anti-EGFR-CAR T cells, and whether this relationship was influenced by NG-347, we directly compared the T cell infiltration scores with a “mouse innate myeloid score” (defined as the geometric mean of mouse-specific probes for Hprt, mF4/80 and mCD11c) across ROIs for both experimental groups

Table 1. Example experimental design for the study depicted in Figure 3.

Test Article 1 Oncolytic Virus (OV, NG-347)		Test Article 2 CAR T cells		
*OV (5E9 vp)	Route of Administrations/Dosing Frequency	CAR-T (82.5%+)	Dose (E6)	Route of Administration/Dosing Frequency
Vehicle		Vehicle	N/A	
Vehicle		EGFR CAR	25.2	
NG-347		EGFR CAR	25.2	
Vehicle	IV; D0 and D3	EGFR CAR	12.6	IV; D6
NG-347		EGFR CAR	12.6	
Vehicle		EGFR CAR	4.2	
NG-347		EGFR CAR	4.2	
NG-347		Vehicle	N/A	
Vehicle		UTD	25.2	
NG-347		UTD	25.2	

(Figure 6h). While no significant relationship was observed for ROIs from tumors collected from mice treated with anti-EGFR-CAR T cell alone (Figure 6h, left), a strong correlation between these variables was observed for ROIs from tumors collected from mice treated with NG-347+ anti-EGFR-CAR T cell (Figure 6h, right), indicating that NG-347 changes to the TME led to joint infiltration of mouse innate cells and human T cells. In sum, in order for robust T cell recruitment and activation to occur in the A549 tumor xenograft TME we hypothesize a 3 stage model: a) T-SIGn virus-mediated reprogramming of the TME enables initial CAR T cell entry into the tumor b) CAR T cell recognition of their specific antigen to provide Signals 1 and 2 through the CAR, c) the virus transgenes and/or TME reprogramming licenses full functional activation of the CAR T cells (Signal 3) which themselves also produce chemokines, thus initiating a positive feedback loop which results in the recruitment of additional CAR T cells as well as host immune cells to collectively drive tumor regression.

The transgenes encoded by T-SIGn viruses play a critical role in the synergistic anti-tumor activity with anti-EGFR CAR T cells

To understand if the transgenes encoded by NG-347 were critical for the observed anti-tumor synergy with anti-EGFR CAR T cells, A549 tumor-bearing NSG mice were treated IV on Days 0 and 3 with the parental T-SIGn virus enadenotucirev (no transgenes), NG-347 or NG-641 (a different T-SIGn virus which encodes transgenes for an anti-human FAP bispecific T-cell activator [FAP-Tac], CXCL9, CXCL10 and IFN α). Note that the FAP-Tac does not bind to mouse FAP so is not expected to be functional in mouse tumor xenograft models.²⁹ Tumor-bearing satellite animals from the vehicle control, enadenotucirev, NG-347 and NG-641 treatment groups were euthanized on Day 6 and their tumor xenografts collected to compare the mRNA transcript expression pattern associated with virus treatment. Either vehicle, untransduced T cells or anti-EGFR CAR T cells were then dosed on Day 6 and tumor volume was monitored bi-weekly (Figure 7a). In this experiment, a suboptimal dose of anti-EGFR CAR T cells was selected (4×10^6 cells/animal), based upon the previous

experiments, that should impact but not fully clear the tumor in combination with the T-SIGn viruses. This sub-optimal CAR T dose was selected to allow us to compare the synergistic effect of the different viruses at a dosage of CAR T cells that would not lead to complete clearance of the tumors. Treatment of animals with the various T-SIGn viruses (enadenotucirev, NG-347 or NG-641) as single agents significantly inhibited A549 tumor growth as compared to the vehicle control, but there was no significant difference between virus treatment groups (Figure 7b, Panel a). The combination of the various T-SIGn viruses + UTD cells significantly inhibited tumor growth as compared to the vehicle control, and the degree of tumor growth inhibition was similar to treatment with the viruses as sole agents. Once again, there was no significant difference between the T-SIGn virus + UTD treatment groups (Figure 7b, Panel b). Interestingly, the combination of NG-347 + anti-EGFR CAR T cells was significantly more effective at reducing the A549 tumor burden than the combination of enadenotucirev + anti-EGFR CAR T cells (Figure 7b, Panel c). Likewise, the combination of NG-641 + anti-EGFR CAR T cells was significantly more effective at reducing the A549 tumor burden than the combination of enadenotucirev + anti-EGFR CAR T cells (Figure 7b, Panel d). It is interesting to note that the NG-347 combination appeared to be slightly more effective than the NG-641 combination (Figure 7b, Panels c vs d). Further, bulk Nanostring nCounter mRNA expression analysis of A549 tumors on Day 6 following treatment with the three viruses demonstrated upregulation of IFN response genes and antigen processing and presentation mRNAs (Figure 7c). Representative example graphs are shown in Figure 7d-e. Although enadenotucirev promoted some increase in expression of each of these genes as compared to the vehicle control group, both NG-347 and NG-641 substantially increased the levels of these mRNAs. As IFN α is the transgene common to both NG-347 and NG-641, it is interesting to speculate that the inclusion of IFN α is critical for the observed anti-tumor synergy when these viruses are used in combination with anti-EGFR CAR T cells. There were some differences in gene expression levels between NG-347 and NG-641, as illustrated by four chemokine genes in figure 7f.

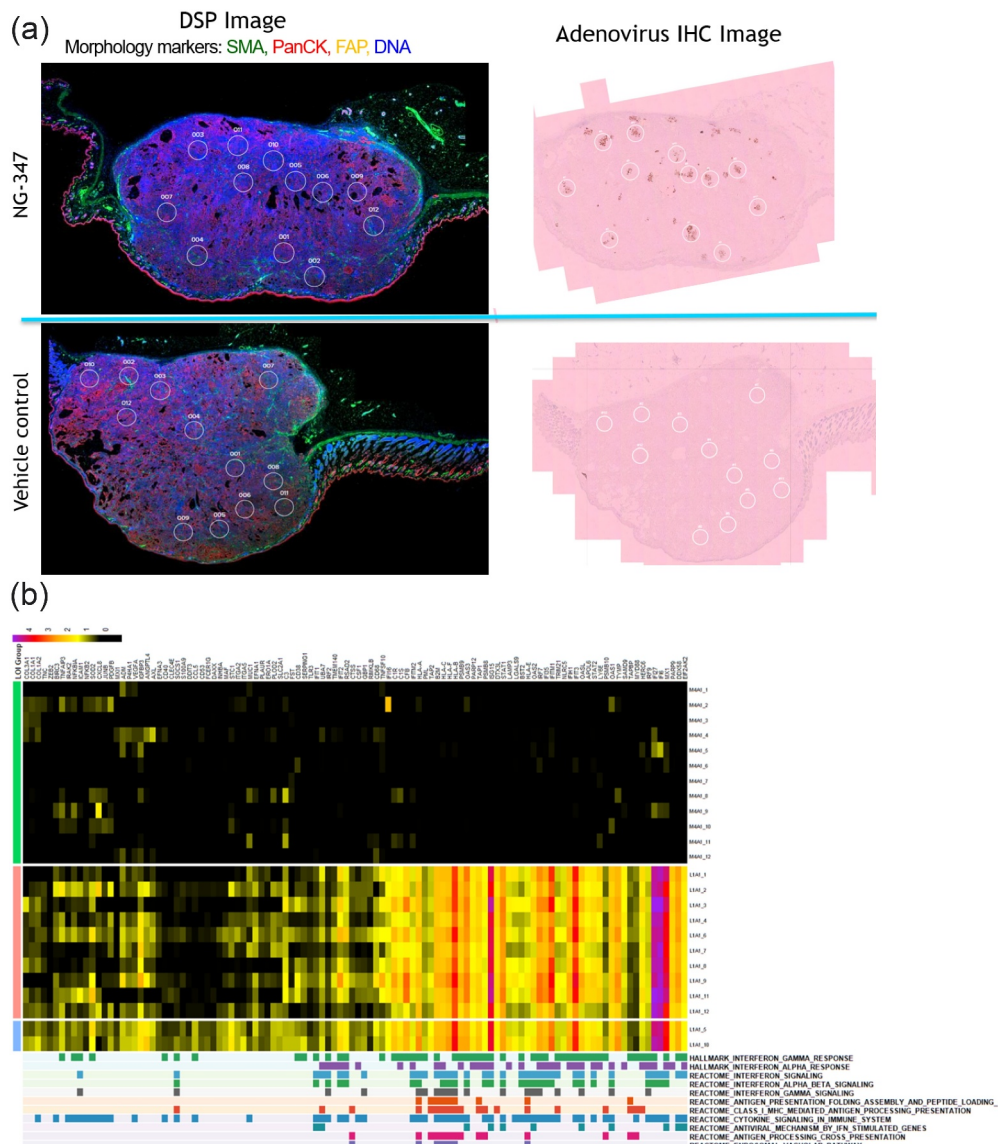


Figure 4. T-SIGN virus NG-347 “re-programs” the A549 TME to a proinflammatory state. a) Serial tissue sections of the NG-347+ and control satellite tumors from the study above were stained via IHC to detect adenoviral capsid (upper and lower right panels) and via immunofluorescence (IF) to detect smooth muscle actin (green), pan-cytokeratin (red), fibroblast activation protein alpha (FAP) and a DAPI DNA counterstain for tissue orientation (upper and lower left panels). We used the viral capsid IHC-stained slide from the NG-347-treated animal as a guide to select 12 adenovirus + regions of interest (ROI) (upper right panel) and then digitally copied those ROIs to the IF-stained serial section used for Digital Spatial Profiling (DSP) mRNA collection (upper left panel). Likewise, we selected 12 random ROIs from the control tumor stained via IHC for viral capsid (lower right panel) and then digitally copied those ROIs to the IF-stained serial section used for DSP mRNA collection (lower left panel). Each ROI was subsequently evaluated for the expression of ~1800 mRNAs detected by the Nanostring GeoMx Cancer Transcriptome Atlas (CTA) RNA detection probes. b) Differential expression analysis identified 110 genes that were positively associated with NG-347 viral replication ($FDR < 0.05$ & $|\log_2(\text{fold-change})| > 0.5$). Interferon response, antigen processing and presentation, cytokine signaling, hypoxia, and other pathways were significantly over-represented in this gene set ($FDR < 0.01$). The heatmap shows expression of these genes (columns) across ROIs (rows) relative to average expression in the control ROIs. The color bar column on the left indicates the ROI groups: green = control tumor xenograft, blue = ROIs from the NG-347 treated tumor xenograft that exhibited high CCL3 and CD80 NG-347 transgene expression, pink = remaining ROIs from the NG-347 treated tumor xenograft. The color bar rows on the bottom indicate which genes are associated with particular over-represented pathways.

The T-SIGN virus NG-347 synergizes with anti-HER-2 CAR T cells to clear subcutaneous A549 tumors

To determine if NG-347 would similarly synergize with CAR T cells targeting a different tumor antigen, we employed CAR T cells specific for the human epithelial cancer antigen HER-2. First, we verified that the HER-2 CAR T cells were selectively able to kill HER-2-expressing A549 tumor cells, but not mouse CT26 tumor cells (not expressing the human HER2 protein) (Figure S9). As a control, anti-CD3/anti-CD28-activated untransduced T cells (UTD) had no significant *in vitro* cytotoxicity against any of the tested tumor cell lines (Figure S9).

Next, A549 tumor-bearing NSG mice were treated IV with NG-347 or vehicle on Days 0 and 3 and then treated with anti-HER-2 CAR T cells or vehicle on Day 6. (see Figure 3a). As seen in the studies with anti-EGFR CAR T cells, NG-347 used as a sole agent significantly impacted tumor growth, but did not clear the tumors (Figure 8, Panel b). However, as we previously demonstrated with anti-EGFR CAR T cells, the combination of NG-347 + anti-HER2 CAR T cells synergized to significantly reduce A549 tumor size as compared to either virus or anti-HER2 CAR T cells when used as a sole agent (Figure 8, Panels c and d). Thus, these data imply that the

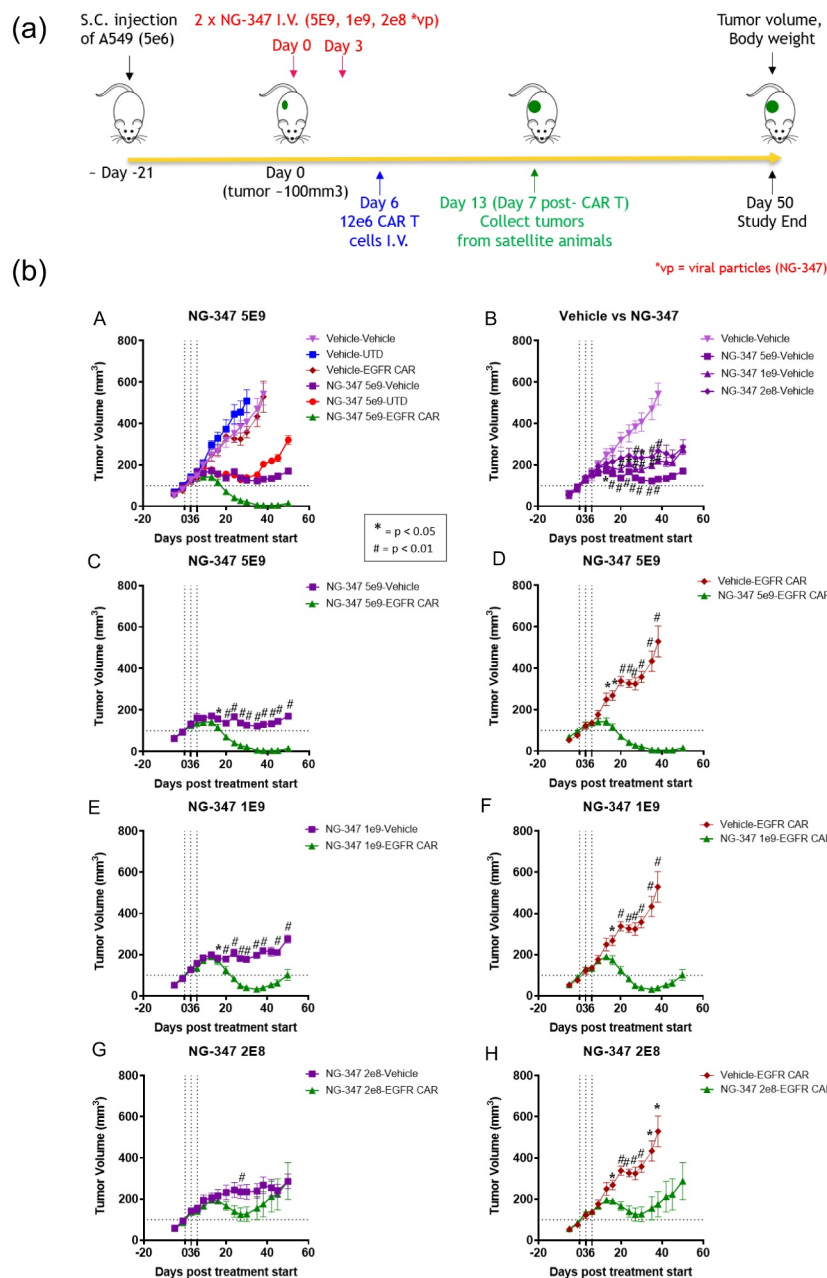


Figure 5. The synergistic anti-tumor effect of NG-347 + anti-EGFR CAR T cells is dependent upon virus dose. a) During this study, we held the CAR T cell dose constant (12×10^6 cells/mouse) and varied the dose of NG-347 (5×10^9 , 1×10^9 or 2×10^8 NG virus particles/mouse; high, medium and low-dose virus cohorts, respectively). We included additional satellite animals in the vehicle alone, vehicle + untransduced T cells (UTD), vehicle + anti-EGFR CAR T cells, and the high dose virus cohort groups including NG-347 alone, NG-347 + UTD cells and NG-347 + anti-EGFR CAR T cells, which were collected on Day 13, one week after administration of the CAR T cells for additional analysis. b) The synergistic anti-tumor effect of NG-347 + anti-EGFR CAR T cells is dependent upon virus dose (complete data from animals treated with high dose NG-347 and/or anti-EGFR CAR T or UTD cells and controls is presented in Panel A). Panel B shows the virus dose-dependent impact of NG-347 on tumor growth. Panels C-D show paired treatment comparisons of high dose NG-347 combined with anti-EGFR CAR T cells vs NG-347 alone or vs anti-EGFR CAR T alone, respectively; Panels E-F show paired treatment comparisons of medium dose NG-347 combined with anti-EGFR CAR T cells vs NG-347 alone or vs anti-EGFR CAR T alone, respectively; Panels G-H show paired treatment comparisons of low dose NG-347 combined with anti-EGFR CAR T cells vs NG-347 alone or vs anti-EGFR CAR T alone, respectively. Symbols indicate significance level from one-sided t-test comparing the indicated groups: *, # indicate $p < .05$ or 0.01 , respectively.

synergy between NG-347 and CAR T cells is not target-dependent and may be a general principle in the A549 model of lung cancer. It is interesting to speculate that T-SIGn viruses may also synergize with multivalent CAR T cells in this model and in human patients with solid tumors.

Discussion

The mere presence of a tumor suggests that the tumor has already defeated the patient's immune system. The immunosuppressive TME thus formed serves as a formidable barrier to any adaptive immune response that the patient's immune

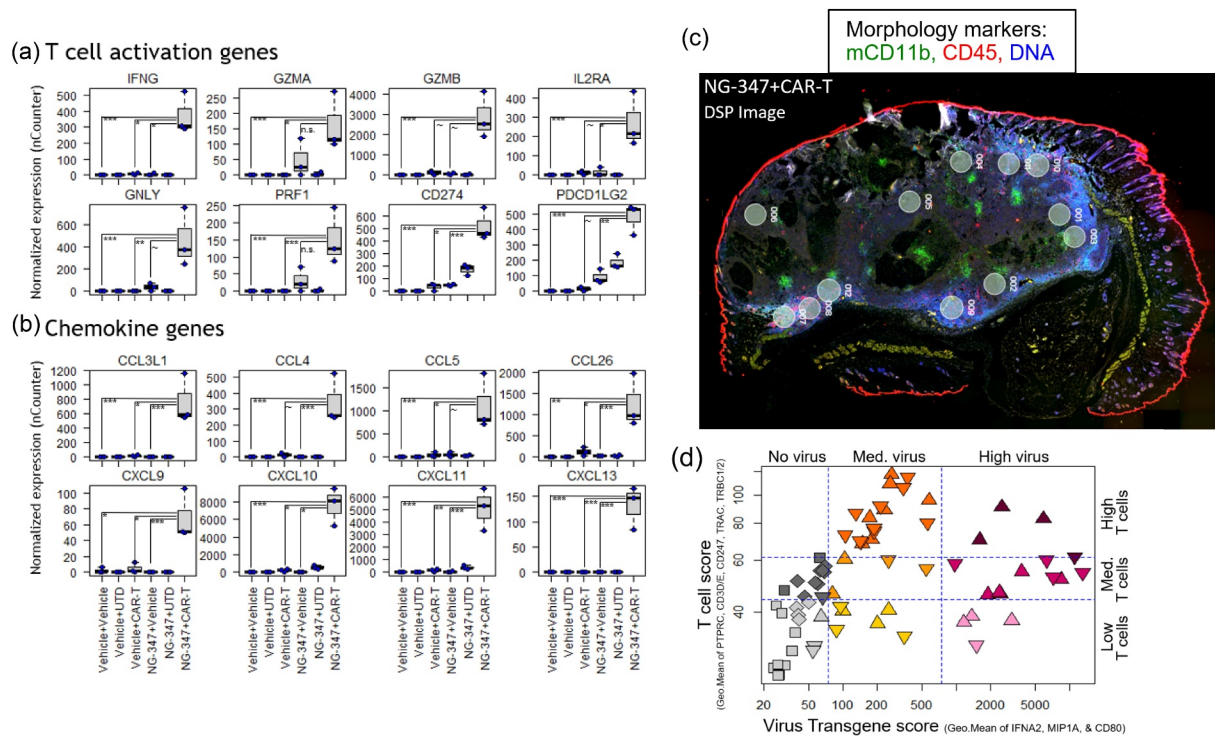


Figure 6. NG-347 enhances the recruitment and activation of anti-EGFR CAR T cells resulting in their improved efficacy against A549 tumors. a-b) Nanostring nCounter gene expression profiling of mRNA extracted from Day 13 tumor FFPE sections of tumors collected from mice treated with vehicle alone, vehicle + untransduced T cells (UTD), vehicle + anti-EGFR CAR T cells, and the high dose virus cohort groups including NG-347 alone, NG-347 + UTD cells and NG-347 + anti-EGFR CAR T cell groups collected on Day 13 were stained via IHC to detect adenoviral capsid (not shown) and serial sections were stained via IF to detect human CD45, murine CD11b and DAPI. As described in the previous DSP experiment, for the animals treated with NG-347, we used the images of tumor sections stained for adenovirus nucleocapsid via IHC to identify ROIs containing virus (not shown) and digitally transferred those ROIs to the corresponding serial IF-stained slide. We attempted to collect ROIs that contained various combinations of virus and/or human CD45 cells and/or murine CD11b cells. We repeated this process on the images of the tissue sections from animals treated with vehicle + anti-EGFR (not shown), and then subjected both groups of samples to Digital Spatial Profiling (DSP) transcriptional analysis. Shown is an example IF-stained slide. d) ROIs from FFPE specimens derived from tumors collected from two mice treated with CAR T cell alone and two mice treated with NG-347+ CAR T cells were scored in terms of T cell signature expression (mean log₂ expression of: PTPRC, CD247, CD3D, CD3E, TRAC, and TRBC1/2) and NG-347 transgene expression (mean log₂ expression of: IFNA2, CCL3, and CD80). In this scatterplot, the T cell score (y axis) is plotted against the virus transgene score (x axis) for all ROIs, which are further categorized into three discrete levels for each factor. Endogenous expression of NG-347 transgenes in the CAR T cells alone ROIs was used to set the background level for the “No virus” group. High levels for the T cell score were only observed for NG-347 + anti-EGFR CAR T cell specimens. Colors represent specific categories for T cell score and virus transgene score. Squares and diamonds indicate ROIs from two biological replicate specimens from mice treated with anti-EGFR CAR T cells alone; triangles and upside-down triangles indicate ROIs from two biological replicate NG-347 + anti-EGFR CAR T cell specimens. e-g) ROI groupings defined in (d) were used to assess how NG-347 modulated immune activation signatures within the tumor. Gene expression levels of cytotoxic T cell effector markers Granzyme-B and Granulysin in ROIs are shown in e and these levels relative to the T cell signature score are shown in f. Murine innate immune cell markers CD11c (DC marker) and F4/80 (macrophage marker) expression levels in ROIs are shown in g. For e-g: symbols indicate significance level from Mixed-Model ANOVA testing for an effect of T cell infiltration level on gene expression (solid lines) or for an interaction between T cell infiltration and transgene expression (dashed lines). Key to significance symbols: ~, *, **, **** indicate $p < .1$ (trend), 0.05, 0.01, or 0.001, respectively. h) The extent of intratumoral murine immune cell infiltration (measured by mean log₂ expression of mouse-specific probes Itgax(mCd11c), Adgr1(F4/80) and Hpvt) was correlated with the extent of intratumor T cell infiltration (measured by T cell score) in tumor xenografts from mice treated with CAR T cells + NG-347 or tumor xenografts from mice treated with CAR T cells alone. Spearman rank correlation statistics are shown.

system may attempt to mount as well as any attempts at adoptive immunotherapy. Here we showed that pre-treatment of immunodeficient NSG mice bearing A549 human tumor xenografts with the T-SIGn oncolytic viral vector NG-347 led to expression of the encoded IFN α , MIP1 α and CD80 transgenes and that the virus “reprogrammed” the TME to a pro-inflammatory state characterized by upregulation of mRNAs which map to pathways associated with acute inflammation. Thus, treatment with NG-347 as a sole therapy prepared the A549 TME to be receptive to incoming immune cells. Further, we showed that there was upregulation of mRNAs associated with antigen presentation and cross-presentation pathways and upregulation of MHC molecules. Thus, with the combined effects of viral tumor cell lysis, release of tumor

neoantigens and upregulation of the antigen processing and presentation machinery, the post-NG-347 TME should be ideal for the activation and recruitment of additional cohorts of anti-tumor T cells via epitope spreading. Indeed, epitope spreading has been shown to be an important element of tumor clearance following therapy with oncolytic viruses.^{30,46–48}

Two of the biggest barriers to effective CAR T cell treatment of solid tumors include ineffective CAR T cell trafficking to the tumor and CAR T cell dysfunction within the hostile TME.⁴⁹ Here we showed that doses of the T-SIGn virus NG-347 and EGFR or HER2 specific CAR T cells, which were sub-therapeutic individually, synergized when combined to clear A549 tumors and pulmonary metastases. We showed that this synergistic anti-tumor effect was dependent upon the transgenes carried by the

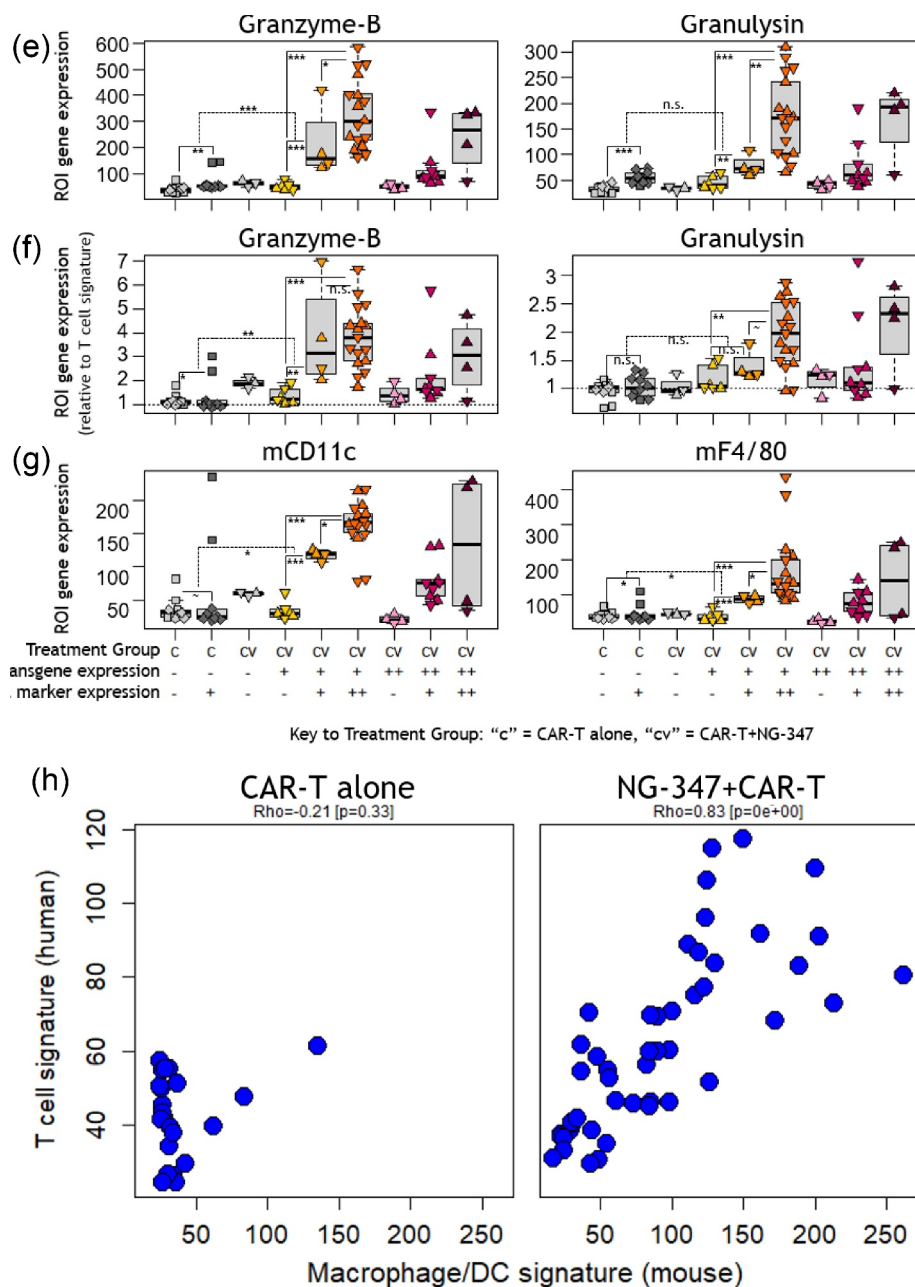


Figure 6 b. Continued

T-SIGn vectors as synergy was not observed when we substituted in the parental virus which lacks transgenes, indicating that TME reprogramming by virus infection and oncolysis alone is not sufficient for supporting anti-tumor efficacy of CAR T cell therapy. We also showed that the combined therapy, but not individual treatments resulted in robust up-regulation of chemokines in the TME. Finally, we showed that within the TME of animals treated with combination therapy, the NG-347 viral load was proportional to human CAR T cell and mouse myeloid cell presence in the TME, as assessed by gene expression analysis, indicating an increased CAR T cell recruitment and/or proliferation in the tumor site, as well as an enhanced mouse macrophage and DC recruitment. Thus, in addition to reprogramming the TME to receive therapeutic CAR T cells and promoting

upregulation of antigen processing and presentation machinery, NG-347 promoted the recruitment and activation of effector T cells which contributed to tumor control.

Our results are similar to a previous combination therapy study in which intra-tumoral (IT) pretreatment with an oncolytic adenovirus encoding RANTES and IL-15 resulted in the recruitment and survival of IV dosed anti-GD2 CAR T cells to the TME of neuroblastoma xenografts, though in that study the combination of virus and CAR T cells did not lead to tumor clearance.²³ Oncolytic viruses are frequently administered via the IT route because they often cannot survive in blood.⁵⁰ Viruses administered in this manner do not have the opportunity to directly infect, lyse and reprogram distant metastases. Rather IT injection

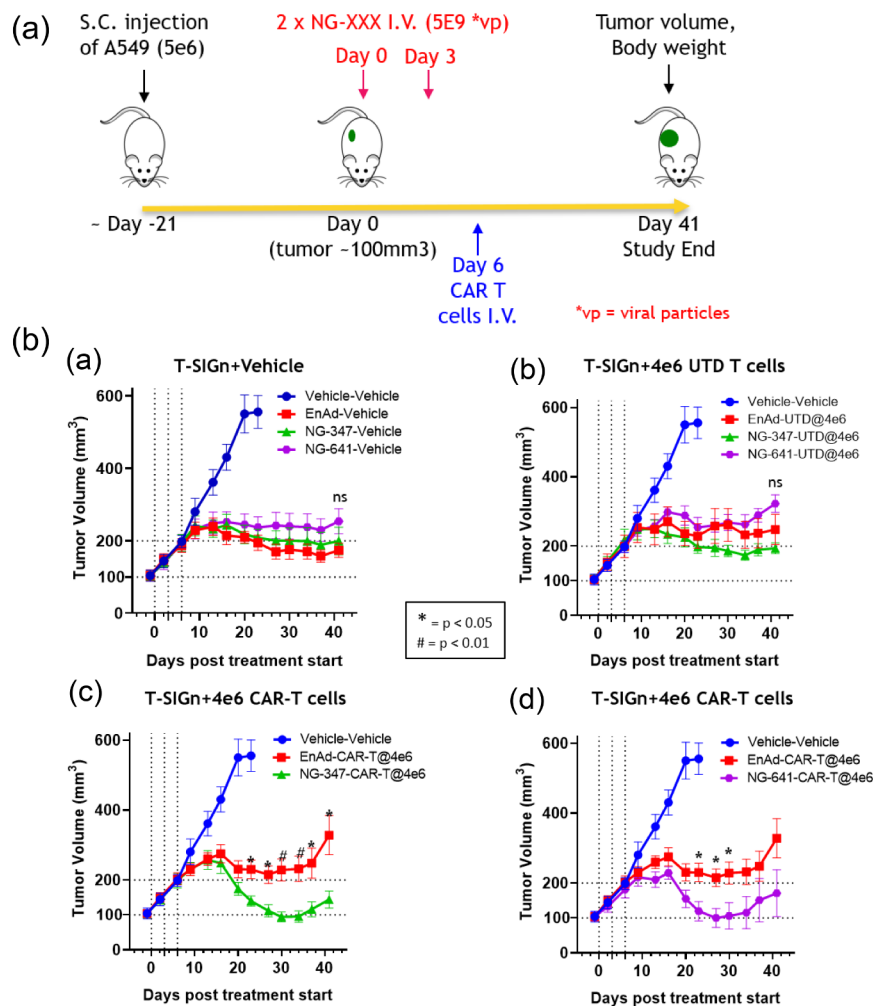


Figure 7. The transgenes encoded by T-SIGn viruses play a critical role in the synergistic anti-tumor activity with anti-EGFR CAR T cells. a) To understand if the transgenes encoded by NG-347 were critical for the observed anti-tumor synergy with anti-EGFR CAR T cells, A549 tumor-bearing NSG mice were treated IV on Days 0 and 3 with the parental T-SIGn virus enadenotucirev (EnAd, no transgenes), NG-347 or NG-641 followed by a suboptimal dose of anti-EGFR CAR T cells (4×10^6 cells/animal) that should not clear the tumor in combination with the T-SIGn viruses. b) Panel a shows the effect of treatment of animals with the various T-SIGn viruses (EnAd, NG-347 or NG-641) as single agents; Panel b shows the effect of combining the various T-SIGn viruses + UTD cells; Panel c shows the effect on tumor growth of the combination of NG-347 + anti-EGFR CAR T cells compared to that of EnAd plus anti-EGFR CAR T cells or vehicle; Panel d shows the effect on tumor growth of the combination of NG-641 + anti-EGFR CAR T cells compared to that of EnAd combined with anti-EGFR CAR T cells or vehicle. Symbols indicate significance level from one-sided t-test comparing the indicated groups: *, # indicate $p < .05$ or 0.01 , respectively. c-f) Nanostring nCounter expression analysis of A549 tumors on Day 6 following treatment with the three viruses, showing mean fold changes of IFN response genes, antigen processing and presentation genes, and other inflammatory mediators (c), with examples of each illustrated in d, e and f, respectively. For d-f: symbols indicate significance level from one-sided t-test comparing the indicated groups: ~, *, **, *** indicate $p < .1$ (trend), 0.05 , 0.01 , or 0.001 , respectively.

is thought to promote an adaptive immune response to tumor neoantigens released by virus-mediated tumor lysis, and it is hypothesized that these tumor neoantigen-specific T cells may traffic to and clear the metastatic lesions, if they express the same neoantigens.⁴⁶ However, enadenotucirev – the T-SIGn vector used to create NG-347 and NG-641 – was actively selected for its stability in blood³² and thus capability of IV dosing.^{33,34} Here we showed that combination therapy with NG-347 and CAR T cells, both dosed via the IV route, cleared both primary A549 human tumor xenografts and cleared/prevented lung metastases at doses that were subtherapeutic when used as individual treatments. Clearance/inhibition of pulmonary metastases was not due to epitope spreading in this study as we used NSG

mice which lack T cells to mount an immune response against tumor neoantigens released via oncolysis. Rather, as we demonstrated via IHC to detect adenovirus capsid protein, NG-347 administered IV traveled directly to and likely reprogrammed the micrometastases, thus preparing them to receive the anti-EGFR CAR T cells. Additionally, activated CAR T cells may have trafficked from the primary tumor to these distant tumor metastatic sites. Thus, in a human patient with an intact immune system, IV dosed combination therapy with T-SIGn viruses followed by CAR T cells may promote clearance of distant metastases by at least three methods: a) direct viral infection of metastatic sites resulting in oncolysis, b) TME reprogramming followed by CAR T cell recruitment and activation and c) by

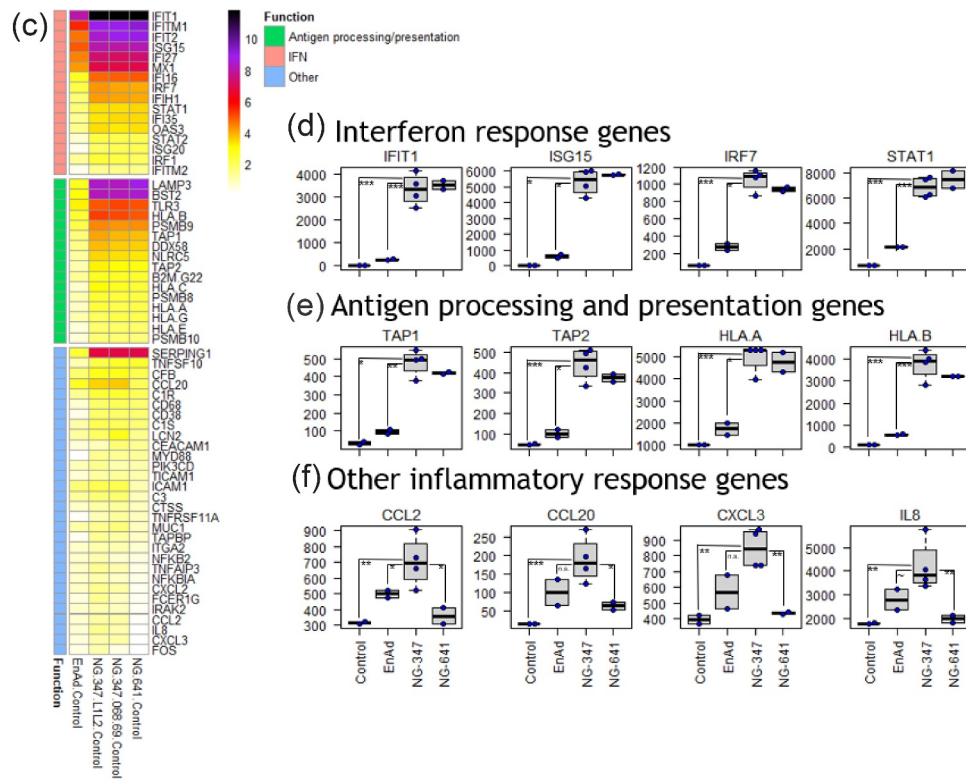


Figure 7 b. Continued

induction of an adaptive anti-tumor immune response to tumor neoantigens released by virolysis (epitope spreading) and recruitment of these cells to the metastatic sites.

One of the most interesting findings in this study was the close correlation between viral burden, human T cell recruitment and mouse innate immune cell recruitment to the TME. We showed

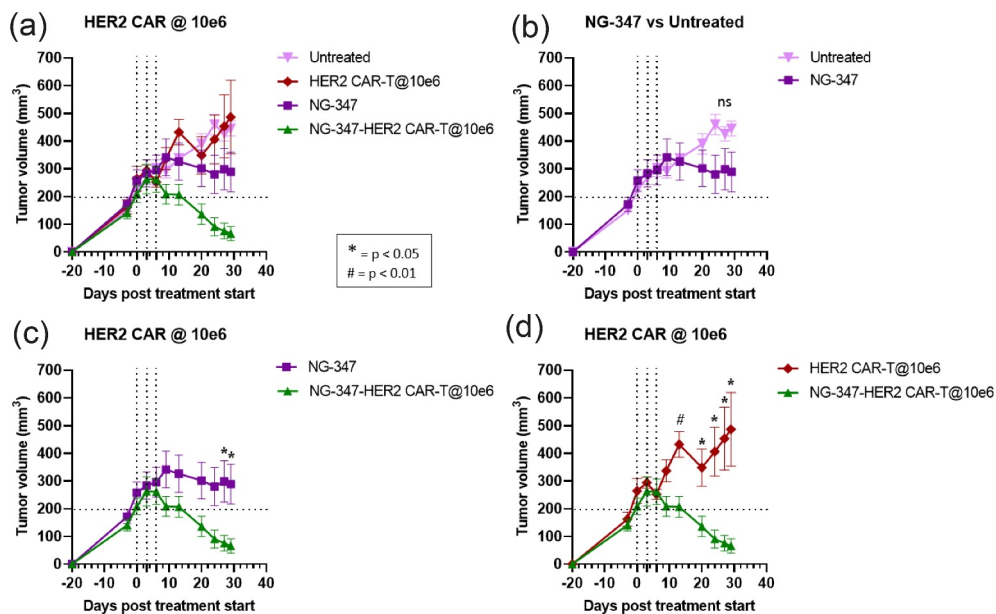


Figure 8. The T-SIGn virus NG-347 synergizes with anti-HER-2 CAR T cells to clear subcutaneous A549 tumors. A549 tumor-bearing NSG mice were treated IV with NG-347 or vehicle on Days 0 and 3 and then treated with anti-HER-2 CAR T cells or vehicle on Day 6 (Study design similar to Figure 3a; composite data presented in Panel a). Panel b compares the effect of NG-347 alone with that of vehicle treatment; Panels c and d show the effect of NG-347 combined with anti-HER2 CAR T cells with NG-347 only or anti-HER2 CAR T cells only treatments, respectively. Symbols indicate significance level from one-sided t-test comparing the indicated groups: *, # indicate $p < .05$ or 0.01 , respectively.

that as the viral burden in a region of the tumor increases, the T cell infiltration also increases (up to a point and then seems to level off or decrease). The decrease in T cell infiltration in regions of the highest virus load is likely artifactual because the latter are characterized by necrosis and cell debris rather than inflammatory cell infiltration. We also showed that mouse innate immune cells are most numerous in regions of the tumor that contain a high number of activated T cells and that enhanced recruitment of both cell populations is associated with the expression of chemokine genes. It is interesting to speculate that the virus-encoded transgenes initially "re-program" the TME to promote recruitment of the first wave of CAR T cells. Upon engagement of their target (EGFR), the CAR T cells then become activated through the CAR (Signals 1 and 2) and produce cytokines, which would fully activate the CAR T cells (Signal 3) and simultaneously recruit the next wave of CAR T cells and innate immune cells to the local TME vicinity. It is possible and likely that the recruited mouse innate immune cells are activated by the human cytokines/chemokines and may or may not contribute to further CAR T cell recruitment. In a human patient, the innate immune cells in the TME would be expected to respond to the released cytokines by becoming activated and producing chemokines and other pro-inflammatory molecules as well. This pattern of CAR T cell recruitment, antigen-specific activation followed by innate cell recruitment and activation followed by more CAR T cell and innate cell recruitment has the potential to form a positive feedback loop, which could potentially persist as long as the antigen for which the CAR T cells are specific is present in the TME.

In summary, our data shows that transgene-expressing T-SIGN oncolytic viral vectors can be effectively administered via the intravenous route and synergize with CAR T cells to eliminate primary tumors and their pulmonary metastases. The viruses effectively "re-program" the TME from an immunosuppressive to a pro-inflammatory microenvironment, thus preparing the tumor to attract and activate CAR T cells and innate antigen presenting cells. The resultant tumor lysis, release of tumor neoantigens and upregulation of antigen processing and presentation machinery should make this environment ideal for the promotion of epitope spreading, thus further amplifying the anti-tumor response.

One caveat is that the A549 tumor xenograft model is an artificial system and lacks certain TME elements which would be found in human patients, such as regulatory T cells and human innate immune cells, which may further contribute to immunosuppression. However, the system also lacks human antigen presenting cells in the TME which could process and present tumor antigen, particularly neoepitopes released from the tumors, and simulate an adaptive anti-tumor immune response that could further contribute to tumor rejection. Thus, the results summarized in this study may or may not translate to clinical efficacy in human patients. In summary, the combination of tumor reprogramming vectors with CAR T cells may be critical to successful treatment of solid tumors.

Acknowledgments

The authors wish to acknowledge the valuable contributions of the bluebird bio Comparative Pathology Laboratory staff including Ken Ganley, Shelby LaBarre and Gina Scarglia, and in vivo Study Leads Anita

Venkitaraman and Christina Ferren. We also thank Dr. Philip Gregory for his critical review of this manuscript.

Disclosure statement

The authors are full-time employees of either bluebird bio or PsiOxus Therapeutics and own equity in their respective companies.

Funding

The author(s) reported that the work featured in this article was fully funded by the two companies.

ORCID

Olmo Sonzogni  <http://orcid.org/0000-0001-5697-8102>

James B. Rottman  <http://orcid.org/0000-0002-3593-6699>

References

- Porter DL, Levine BL, Kalos M, Bagg A, June CH. Chimeric antigen receptor-modified T cells in chronic lymphoid leukemia. *N Engl J Med.* 2011;365(8):725–733. doi:10.1056/NEJMoa1103849.
- Grupp SA, Kalos M, Barrett D, Aplenc R, Porter DL, Rheingold SR, Teachey DT, Chew A, Hauck B, Wright JF, et al. Chimeric antigen receptor-modified T cells for acute lymphoid leukemia. *N Engl J Med.* 2013;368(16):1509–1518. doi:10.1056/NEJMoa1215134.
- Maude SL, Frey N, Shaw PA, Aplenc R, Barrett DM, Bunin NJ, Chew A, Gonzalez VE, Zheng Z, Lacey SF, et al. Chimeric antigen receptor T cells for sustained remissions in leukemia. *N Engl J Med.* 2014;371(16):1507–1517. doi:10.1056/NEJMoa1407222.
- Fry TJ, Shah NN, Orentas RJ, Stetler-Stevenson M, Yuan CM, Ramakrishna S, Wolters P, Martin S, Delbrook C, Yates B, et al. CD22-targeted CAR T cells induce remission in B-ALL that is naive or resistant to CD19-targeted CAR immunotherapy. *Nat Med.* 2018;24(1):20–28. doi:10.1038/nm.4441.
- Gardner RA, Finney O, Annesley C, Brakke H, Summers C, Leger K, Bleakley M, Brown C, Mgebroff S, Kelly-Spratt KS, et al. Intent-to-treat leukemia remission by CD19 CAR T cells of defined formulation and dose in children and young adults. *Blood.* 2017;129(25):3322–3331. doi:10.1182/blood-2017-02-769208.
- Ramos CA, Grover NS, Beaven AW, Lulla PD, Wu M-F, Ivanova A, Wang T, Shea TC, Rooney CM, Dittus C, et al. Anti-CD30 CAR-T cell therapy in relapsed and refractory hodgkin lymphoma. *J Clin Oncol.* 2020;38(32):3794–3804. doi:10.1200/JCO.20.01342.
- Ramos CA, Savoldo B, Torrano V, Ballard B, Zhang H, Dakhova O, Liu E, Carrum G, Kamble RT, Gee AP, et al. Clinical responses with T lymphocytes targeting malignancy-associated kappa light chains. *J Clin Invest.* 2016;126(7):2588–2596. doi:10.1172/JCI86000.
- Raje N, Berdeja J, Lin Y, Siegel D, Jagannath S, Madduri D, Liedtke M, Rosenblatt J, Maus MV, Turka A, et al. Anti-BCMA CAR T-cell therapy bb2121 in relapsed or refractory multiple myeloma. *N Engl J Med.* 2019;380(18):1726–1737. doi:10.1056/NEJMoa1817226.
- Turtle CJ, Hanafi L-A, Berger C, Hudecek M, Pender B, Robinson E, Hawkins R, Chaney C, Chierian S, Chen X, et al. Immunotherapy of non-hodgkin's lymphoma with a defined ratio of CD8+ and CD4+CD19-specific chimeric antigen receptor-modified T cells. *Sci Transl Med.* 2016;8(355):355ra116. doi:10.1126/scitranslmed.aaf8621.
- Kochenderfer JN, Somerville RPT, Lu T, Yang JC, Sherry RM, Feldman SA, McIntyre L, Bot A, Rossi J, Lam N, et al. Long-duration complete remissions of diffuse large B cell lymphoma after Anti-CD19 chimeric antigen receptor T cell therapy. *Mol Ther.* 2017;25(10):2245–2253. doi:10.1016/j.ymthe.2017.07.004.
- Majzner RG, Mackall CL. Clinical lessons learned from the first leg of the CAR T cell journey. *Nat Med.* 2019;25(9):1341–1355. doi:10.1038/s41591-019-0564-6.

12. Holstein SA, Lunning MA. CAR T-cell therapy in hematologic malignancies: a voyage in progress. *Clin Pharmacol Ther.* 2020;107(1):112–122. doi:10.1002/cpt.1674.
13. Boyiadzis MM, Dhodapkar MV, Brentjens RJ, Kochenderfer JN, Neelapu SS, Maus MV, Porter DL, Maloney DG, Grupp SA, Mackall CL, et al. Chimeric antigen receptor (CAR) T therapies for the treatment of hematologic malignancies: clinical perspective and significance. *J Immunother Cancer.* 2018;6(1):137. doi:10.1186/s40425-018-0460-5.
14. Sadeqi Nezhad M, Yazdanifar M, Abdollahpour-Alitappeh M, Sattari A, Seifalian A, Bagheri N. Strengthening the CAR-T cell therapeutic application using CRISPR/Cas9 technology. *Biotechnol Bioeng.* 2021;118(10):3691–3705. doi:10.1002/bit.27882.
15. Wagner J, Wickman E, DeRenzo C, Gottschalk S. CAR T cell therapy for solid tumors: bright future or dark reality? *Mol Ther.* 2020;28(11):2320–2339. doi:10.1016/j.ymthe.2020.09.015.
16. Louis CU, Savoldo B, Dotti G, Pule M, Yvon E, Myers GD, Rossig C, Russell HV, Diouf O, Liu E, et al. Antitumor activity and long-term fate of chimeric antigen receptor-positive T cells in patients with neuroblastoma. *Blood.* 2011;118(23):6050–6056. doi:10.1182/blood-2011-05-354449.
17. Ahmed N, Brawley VS, Hegde M, Robertson C, Ghazi A, Gerken C, Liu E, Dakhova O, Ashoori A, Corder A, et al. human epidermal growth factor receptor 2 (HER2) -specific chimeric antigen receptor-modified T cells for the immunotherapy of HER2-positive sarcoma. *J Clin Oncol.* 2015;33(15):1688–1696. doi:10.1200/JCO.2014.58.0225.
18. Feng K, Guo Y, Dai H, Wang Y, Li X, Jia H, Han W. Chimeric antigen receptor-modified T cells for the immunotherapy of patients with EGFR-expressing advanced relapsed/refractory non-small cell lung cancer. *Sci China Life Sci.* 2016;59(5):468–479. doi:10.1007/s11427-016-5023-8.
19. Newick K, O'Brien S, Moon E, Albelda SM. CAR T cell therapy for solid tumors. *Annu Rev Med.* 2017;68(1):139–152. doi:10.1146/annurev-med-062315-120245.
20. Martinez M, Moon EK. CAR T cells for solid tumors: new strategies for finding, infiltrating, and surviving in the tumor microenvironment. *Front Immunol.* 2019;10:128. doi:10.3389/fimmu.2019.00128.
21. Liu Y, Zugazagoitia J, Ahmed FS, Henick BS, Gettinger SN, Herbst RS, Schalper KA, Rimm DL. Immune cell PD-L1 colocalizes with macrophages and is associated with outcome in PD-1 pathway blockade therapy. *Clin Cancer Res.* 2020;26(4):970–977. doi:10.1158/1078-0432.CCR-19-1040.
22. Ajina A, Maher J. Prospects for combined use of oncolytic viruses and CAR T-cells. *J Immunother Cancer.* 2017;5:90.
23. Nishio N, Diaconu I, Liu H, Cerullo V, Caruana I, Hoyos V, Bouchier-Hayes L, Savoldo B, Dotti G. Armed oncolytic virus enhances immune functions of chimeric antigen receptor-modified T cells in solid tumors. *Cancer Res.* 2014;74(18):2245–2253. doi:10.1158/0008-5472.CAN-14-0697.
24. Porter CE, Rosewell Shaw A, Jung Y, Yip T, Castro PD, Sandulache VC, Sikora A, Gottschalk S, Ittman MM, Brenner MK, et al. Oncolytic adenovirus armed with bite, cytokine, and checkpoint inhibitor enables CAR T cells to control the growth of heterogeneous tumors. *Mol Ther.* 2020;28(5):1251–1262. doi:10.1016/j.ymthe.2020.02.016.
25. Shi T, Song X, Wang Y, Liu F, Wei J. Combining oncolytic viruses with cancer immunotherapy: establishing a new generation of cancer treatment. *Front Immunol.* 2020;11:683. doi:10.3389/fimmu.2020.00683.
26. Felt SA, Moerdyk-Schauwecker MJ, Grdzlishvili VZ. Induction of apoptosis in pancreatic cancer cells by vesicular stomatitis virus. *Virology.* 2015;474:163–173. doi:10.1016/j.virol.2014.10.026.
27. Saha D, Wakimoto H, Rabkin SD. Oncolytic herpes simplex virus interactions with the host immune system. *Curr Opin Virol.* 2016;21:26–34. doi:10.1016/j.coviro.2016.07.007.
28. Park AK, Fong Y, Kim SI, Yang J, Murad JP, Lu J, Jeang B, Chang WC, Chen NG, Thomas SH, et al. Effective combination immunotherapy using oncolytic viruses to deliver CAR targets to solid tumors. *Sci Transl Med.* 2020;12(559). doi:10.1126/scitranslmed.aaz1863.
29. Freedman JD, Duffy MR, Lei-Rossmann J, Muntzer A, Scott EM, Hagel J, Campo L, Bryant RJ, Verrill C, Lambert A, et al. An oncolytic virus expressing a T-cell engager simultaneously targets cancer and immunosuppressive stromal cells. *Cancer Res.* 2018;78(24):6852–6865. doi:10.1158/0008-5472.CAN-18-1750.
30. Moesta AK, Cooke K, Piasecki J, Mitchell P, Rottman JB, Fitzgerald K, Zhan J, Yang B, Le T, Belmontes B, et al. Local Delivery of OncoVEXmGM-CSF generates systemic antitumor immune responses enhanced by cytotoxic T-lymphocyte-associated protein blockade. *Clin Cancer Res.* 2017;23(20):6190–6202. doi:10.1158/1078-0432.CCR-17-0681.
31. Li J, O'Malley M, Sampath P, Kalinski P, Bartlett DL, Thorne SH. Expression of CCL19 from oncolytic vaccinia enhances immunotherapeutic potential while maintaining oncolytic activity. *Neoplasia.* 2012;14(12):1115–1121. doi:10.1593/neo.121272.
32. Di Y, Seymour L, Fisher K. Activity of a group B oncolytic adenovirus (ColoAd1) in whole human blood. *Gene Ther.* 2014;21(4):440–443. doi:10.1038/gt.2014.2.
33. Garcia-Carbonero R, Salazar R, Duran I, Osman-Garcia I, Paz-Ares L, Bozada JM, Boni V, Blanc C, Seymour L, Beadle J, et al. Phase 1 study of intravenous administration of the chimeric adenovirus enadenotucirev in patients undergoing primary tumor resection. *J Immunother Cancer.* 2017;5(1):71. doi:10.1186/s40425-017-0277-7.
34. Machiels JP, Salazar R, Rottey S, Duran I, Dirix L, Geboes K, Wilkinson-Blanc C, Pover G, Alvis S, Champion B, et al. A phase 1 dose escalation study of the oncolytic adenovirus enadenotucirev, administered intravenously to patients with epithelial solid tumors (EVOLVE). *J Immunother Cancer.* 2019;7(1):20. doi:10.1186/s40425-019-0510-7.
35. Illingworth S, Di Y, Bauzon M, Lei J, Duffy MR, Alvis S, Champion B, Lieber A, Hermiston T, Seymour LW, et al. Preclinical safety studies of enadenotucirev, a chimeric group B human-specific oncolytic adenovirus. *Mol Ther Oncolytics.* 2017;5:62–74. doi:10.1016/j.omto.2017.03.003.
36. Challita PM, Skelton D, El-khoueiry A, Yu XJ, Weinberg K, Kohn DB. Multiple modifications in cis elements of the long terminal repeat of retroviral vectors lead to increased expression and decreased DNA methylation in embryonic carcinoma cells. *J Virol.* 1995;69(2):748–755. doi:10.1128/jvi.69.2.748-755.1995.
37. Milone MC, Fish JD, Carpenito C, Carroll RG, Binder GK, Teachey D, Samanta M, Lakhil M, Gloss B, Danet-Desnoyers G, et al. Chimeric receptors containing CD137 signal transduction domains mediate enhanced survival of T cells and increased antileukemic efficacy in vivo. *Mol Ther.* 2009;17(8):1453–1464. doi:10.1038/mt.2009.83.
38. Imai C, Mihara K, Andreansky M, Nicholson IC, Pui C-H, Geiger TL, Campana D. Chimeric receptors with 4-1BB signaling capacity provoke potent cytotoxicity against acute lymphoblastic leukemia. *Leukemia.* 2004;18(4):676–684. doi:10.1038/sj.leu.2403302.
39. Negre O, Bartholomae C, Beuzard Y, Cavazzana M, Christiansen L, Courne C, Deichmann A, Denaro M, de Drouzey E, Finer M, et al. Preclinical evaluation of efficacy and safety of an improved lentiviral vector for the treatment of beta-thalassemia and sickle cell disease. *Curr Gene Ther.* 2015;15(1):64–81. doi:10.2174/1566523214666141127095336.
40. Tomayko MM, Reynolds CP. Determination of subcutaneous tumor size in athymic (nude) mice. *Cancer Chemother Pharmacol.* 1989;24(3):148–154. doi:10.1007/BF00300234.
41. Zollinger DR, Lingle SE, Sorg K, Beechem JM, Merritt CR et al. GeoMx RNA assay: high multiplex, digital, spatial analysis of RNA in FFPE tissue. *Methods Mol Biol.* 2020;2148:331–345.
42. Liberzon A, Birger C, Thorvaldsdóttir H, Ghandi M, Mesirov J, Tamayo P. The molecular signatures database (MSigDB) hallmark gene set collection. *Cell Syst.* 2015;1(6):417–425. doi:10.1016/j.cels.2015.12.004.

43. Jassal B, Matthews L, Viteri G, Gong C, Lorente P, Fabregat A, Sidiropoulos K, Cook J, Gillespie M, Haw R, et al. The reactome pathway knowledgebase. *Nucleic Acids Res.* 2020;48(D1):D498–D503. doi:10.1093/nar/gkz1031.
44. Kanehisa M, Goto S, Sato Y, Furumichi M, Tanabe M. KEGG for integration and interpretation of large-scale molecular data sets. *Nucleic Acids Res.* 2012;40:D109–14. doi:10.1093/nar/gkr988.
45. Marino N, Illingworth S, Kodialbail P, Patel A, Calderon H, Lear R, Fisher KD, Champion BR, Brown ACN, et al. Development of a versatile oncolytic virus platform for local intra-tumoural expression of therapeutic transgenes. *PLoS One.* 2017;12(5):e0177810. doi:10.1371/journal.pone.0177810.
46. Woller N, Gürlevik E, Fleischmann-Mundt B, Schumacher A, Knocke S, Kloos AM, Saborowski M, Geffers R, Manns MP, Wirth TC, et al. viral infection of tumors overcomes resistance to PD-1-immunotherapy by broadening neoantigenome-directed T-cell responses. *Mol Ther.* 2015;23(10):1630–1640. doi:10.1038/mt.2015.115.
47. Tahtinen S, Grönberg-Vähä-Koskela S, Lumen D, Merisalo-Soikkeli M, Siurala M, Airaksinen AJ, Vähä-Koskela M, Hemminki A. Adenovirus improves the efficacy of adoptive T-cell therapy by recruiting immune cells to and promoting their activity at the tumor. *Cancer Immunol Res.* 2015;3(8):915–925. doi:10.1158/2326-6066.CIR-14-0220-T.
48. Kanerva A, Nokisalmi P, Diaconu I, Koski A, Cerullo V, Liikanen I, Tähtinen S, Oksanen M, Heiskanen R, Pesonen S, et al. Antiviral and antitumor T-cell immunity in patients treated with GM-CSF-coding oncolytic adenovirus. *Clin Cancer Res.* 2013;19(10):2734–2744. doi:10.1158/1078-0432.CCR-12-2546.
49. Hui L, Chen Y. Tumor microenvironment: sanctuary of the devil. *Cancer Lett.* 2015;368(1):7–13. doi:10.1016/j.canlet.2015.07.039.
50. Macedo N, Miller DM, Haq R, Kaufman HL. Clinical landscape of oncolytic virus research in 2020. *J Immunother Cancer.* 2020;8(2):e001486. doi:10.1136/jitc-2020-001486.